Homeostatic nuclear RAGE–ATM interaction is essential for efficient DNA repair

Varun Kumar[1,2,†], Thomas Fleming[1,2,†], Stefan Terjung[3], Christian Gorzelanny[4], Christoffer Gebhardt[5,6], Raman Agrawal[7], Marcus A. Mall[7], Julia Ranzinger[8], Martin Zeier[8], Thati Madhusudhan[9], Satish Ranjan[9], Berend Isermann[9], Arthur Liesz[10], Divija Deshpande[1], Hans-Ulrich Häring[2,11], Subrata K Biswas[12], Paul R. Reynolds[13], Hans-Peter Hammes[14], Rainer Peperkok[3], Peter Angel[6], Stephan Herzig[1,2,15,16] and Peter P. Nawroth[1,2,16,*]

[1]Department of Medicine I and Clinical Chemistry, University Hospital of Heidelberg, INF 410, Heidelberg, Germany, [2]German Center for Diabetes Research (DZD), Helmholtz-Zentrum, München, Germany, [3]European Molecular Biology Laboratory, Advanced Light Microscopy Facility, Heidelberg, Germany, [4]Experimental Dermatology, Medical Faculty Mannheim, University of Heidelberg, Mannheim, Germany, [5]Division of Dermatooncology, German Cancer Research Center (DKFZ), Heidelberg, Germany, [6]Division of Signal Transduction and Growth Control DKFZ DKFZ-ZMBH Alliance, German Cancer Research Center (DKFZ), Heidelberg, Germany, [7]Department of Translational Pulmonology, Translational Lung Research Center Heidelberg (TLRC), German Center for Lung Research (DZL), University of Heidelberg, INF 156, Heidelberg, Germany, [8]Department of Nephrology, University of Heidelberg, Heidelberg, INF 410, Heidelberg, Germany, [9]Institute of Clinical Chemistry and Pathobiochemistry, Otto-von-Guericke-University, Magdeburg, Germany, [10]Institute for Stroke and Dementia Research (ISD) University Hospital München, Munich, Germany; Munich Cluster for Systems Neurology (SyNergy), Munich, Germany, [11]Department of Internal Medicine, University of Tübingen, Tübingen, Germany, [12]Department of Biochemistry and Molecular Biology, Bangabandhu Sheikh Mujib Medical University (BSMMU), Shahbag, Dhaka 1000, Bangladesh, [13]Department of Physiology and Developmental Biology, Brigham Young University, 3054 Life Sciences Building, Provo, UT 84602, USA, [14]5th Medical Department, Medical Faculty Mannheim, Heidelberg University, Mannheim, Germany, [15]Institute for Diabetes and Cancer, Helmholtz Center Munich, Neuherberg, Germany and [16]Joint Heidelberg-IDC Translational Diabetes Program, Helmholtz-Zentrum, München, Germany

ABSTRACT

The integrity of genome is a prerequisite for healthy life. Indeed, defects in DNA repair have been associated with several human diseases, including tissue-fibrosis, neurodegeneration and cancer. Despite decades of extensive research, the spatio-mechanical processes of double-strand break (DSB)-repair, especially the auxiliary factor(s) that can stimulate accurate and timely repair, have remained elusive. Here, we report an ATM-kinase dependent, unforeseen function of the nuclear isoform of the Receptor for Advanced Glycation End-products (nRAGE) in DSB-repair. RAGE is phosphorylated at Serine[376] and Serine[389] by the ATM kinase and is recruited to the site of DNA-DSBs *via* an early DNA damage response. nRAGE preferentially co-localized with the MRE11 nuclease subunit of the MRN complex and orchestrates its nucleolytic activity to the ATR kinase signaling. This promotes efficient RPA2[S4-S8] and CHK1[S345] phosphorylation and thereby prevents cellular senescence, IPF and carcinoma formation. Accordingly, loss of RAGE causatively linked to perpetual DSBs signaling, cellular senescence and fibrosis. Importantly, in a mouse model of idiopathic pulmonary fibrosis (RAGE^{−/−}), reconstitution of RAGE efficiently restored DSB-repair and reversed pathological anomalies. Collectively, this study identifies nRAGE as a master regulator of DSB-repair, the absence of which orchestrates persistent DSB signaling to senescence, tissue-fibrosis and oncogenesis.

*To whom correspondence should be addressed. Tel: +49 6221 56 8601; Fax: +49 6221 56 5226; Email: peter.nawroth@med.uni-heidelberg.de
†These authors contributed equally to this work as first authors.

INTRODUCTION

Every cell of the human body encounters tens to thousands of DNA damages every day (1,2), of which DNA-DSBs are the most cytotoxic form of DNA lesions. These lesions, if left unrepaired, lead to various disorders such as cancer, neurodegeneration, fibrosis and immunodeficiency (1,3,4). Normally, cells respond to these breaks by a complex series of events commonly known as the DNA damage response (DDR) which detect, signal and repair DSB by either an error-free homologous recombination repair (HRR) pathway or error-prone non-homologous end joining repair (NHEJ) pathway (5). DSBs lead to the activation of the ATM kinase, which then phosphorylates several downstream targets including the histone variant H2AX and the effector kinase CHK2 (6). Thus, on-demand orchestration of temporal and spatial repair signaling plays an important role in preserving the genetic integrity. Impairment of DNA repair, leading to an accumulation of DNA-DSBs can result in some of the most devastating diseases of the western society, including neurodegeneration, pulmonary fibrosis and cancer.

Homologous recombination repair requires extensive nucleolytic processing of broken DNA ends, commonly known as end-resection (7,8). This repair step generates ssDNA tails (which play an important role for homology search) and is concerted through the action of MRE11 and its associated nucleases, which form a part of the DNA damage sensor complex MRN (MRE11–Rad50–Nbs1) (9). MRE11 possess exo- as well as endonuclease activities, but recombination repair predominantly relies upon MRE11 endonuclease activity (10). However, MRE11 shows exclusively exonuclease activity on a paired dsDNA, until provided with artificial looped or both end-blocked dsDNA templates (10,11). Hence, one of the most important steps in the mechanisms of DNA repair has yet to be fully understood and therefore requires further investigation (12). In the absence of timely repair, persistent DNA damage associated signaling prevails, which drives cells towards an irreversible senescence-associated secretory phenotype (SASP) (13,14), marked by abundant secretion of paracrine active molecules such as IL-6 and IL-8. These cytokines then initiate a traditional inflammatory response (14–16), leading to fibrosis and promotion of oncogenesis.

Persistent DNA damage associated SASP depletes tissue reserves of the stem and progenitor cells, thereby limiting tissue regeneration (17). In addition, an altered paracrine signaling (hallmarked by IL-6, IL-8, IL-1α and IL-1β), leads to the development of permanent fibrotic scars and carcinomas in the affected tissue (18,19). Among all the organs of the body, the lung is profusely exposed to high O_2 tension as well as reactive oxygen species (ROS), and thus always in need of an efficient DNA-repair system to combat the consequences of increased ROS.

The receptor for advanced glycation end-products (RAGE) is a multi-ligand receptor which can bind to various ligands such as advanced glycation end-products (AGEs), originated from oxidative modifications of cellular biomolecules, S100 protein family members, glycosaminoglycans, amyloid β-peptides, high-mobility group box-1 (HMGB1) and nucleic acids (20). The RAGE-ligand

interaction leads to the activation of MAP kinase signaling pathway. Further ligand-induced up-regulation of RAGE is also known in various patho-physiological situations including late diabetic complications, Alzheimer disease and several other neurodegenerative diseases (21,22). Within the lungs, the pattern recognition receptor RAGE is the fifth-most abundant protein and, more importantly, nuclear accumulation of this receptor has been observed in different tissues and several diseases associated with loss of genomic integrity (23–25). Others have reported that pattern recognition receptors are involved in DNA repair (26–28). This suggests that within the nucleus RAGE might not serve as a cell surface pattern recognition receptor for AGEs, S100-proteins, amyloid-β-peptides and others (29). Therefore, RAGE in the nucleus might function differently from that of surface RAGE. The physiological relevance of RAGE in the nucleus is hitherto unknown. Similar to ATM deficient murine models of ataxia telangiectasia (30,31) or persistent DSB signaling models (32–35), loss of RAGE affects pulmonary repair mechanisms resulting in pulmonary fibrosis (29,36,37) and other defective DNA DSB repair associated anomalies. Thus, the study of the physiological role of RAGE in the nucleus might help to understand not only steps critical for DNA repair, but also to unravel the connection between DNA repair, senescence and fibrosis.

In this study, we demonstrate that RAGE is recruited to the site of DNA damage *via* an ATM signaling cascade and there it modulates the nucleolytic activity of the MRE11 nuclease for long range end-resection, orchestrates timely regulation of ATM to ATR switch for efficient DNA-repair. By doing so, ATM-phosphorylated nuclear RAGE prevents cellular senescence, inflammation, pulmonary fibrosis and cancer. Collectively, our study provides novel mechanistic insights into DNA end-resection and identifies RAGE as a homeostatic regulator of DNA-DSB repair.

MATERIALS AND METHODS

Details on plasmid construction and antibodies used, DNA damage treatment, immunofluorescence staining, immunoprecipitation, cell culture, whole body irradiation, proliferation assay, FACS, Comet assay, expression of recombinant proteins, Ni-NTA pull down assay, virus production and information on oligo(s) used in this study are described in supplementary methods.

Mouse models

All the experimental procedures were carried out in two different mouse strains: The wild type (WT) and RAGE knock out (RAGE$^{-/-}$). WT mice (C57BL6) were obtained from Charles River, Boston USA. RAGE$^{-/-}$ mice were created by us in light of a SVEV129 and backcrossed more than ten times with C57BL6 mice (38). The procedure of the experiments was approved by the animal care and use committees at the Regierungspräsidium Tübingen and Karlsruhe, Germany (35-9185.81/G-90/0435-9185.81/G-182/08, renal reperfusion injury: Animal permit number: G-16/10, brain reperfusion injury: animal permit number: Az.222-2013).

Purification of ultrapure tissue organelles

The tissue fractionation was performed as described (39). Briefly, lung tissue was rinsed twice in ice cold phosphate-buffered saline (PBS) and homogenized in ice-cold lysis buffer 250 STM DPS containing 250 mM sucrose, 50 mM Tris–HCl (pH 7.4), 5 mM $MgCl_2$, 1 mM DTT, 25 μg/ml Spermine, 25 μg/ml Spermidine, 1 mM PMSF and EDTA free complete protease inhibitor cocktail (Roche) using a tight fitting Teflon pestle. The lysate was centrifuged in a bench-top centrifuge at 800 g for 15 min; the supernatant served as source for cytosol, mitochondria and microsomes. The soluble mitochondrial proteins were extracted using ice cold hypotonic HDP buffer (10 mM HEPES (pH 7.9), 1 mM DTT, 1 mM PMSF and other protease inhibitors for 30 min on ice, briefly sonicated and the debris pelleted at 13 000 rpm for 30 min. Membrane bound mitochondrial proteins and microsomal proteins were extracted using ME buffer (20 mM Tris–HCl (pH 7.8), 0.4M NaCl, 15% glycerol, 1mM DTT, 1.5% Triton X-100, 1 mM PMSF and other protease inhibitors for 30 min on ice, briefly sonicated and the debris pelleted at 13 000 rpm for 30 min. The pellet, which contains the nuclei was re-homogenized in lysis buffer and centrifuged as above. The nuclei were resuspended in 2 M STM-DPS buffer (2 M sucrose, 50 mM Tris–HCl (pH 7.4), 5 mM $MgCl_2$, 1 mM DTT 25 μg/ml Spermine, 25 μg/ml Spermidine, 1 mM PMSF and EDTA free complete protease inhibitor cocktail (Roche)) and pelleted by ultracentrifugation at 80 000 g in a SW40Ti (Beckman) for 45 min. Mitochondria were isolated from the crude cytoplasmic fraction by bench-top centrifugation at 6000g for 15 min. The mitochondrial pellet was washed and pelleted twice in lysis buffer. The cytosolic fraction was obtained after removal of the microsomal fraction by ultracentrifugation at 100 000g in a SW60Ti (Beckman) for 1 h. Nuclear proteins were extracted by re-suspending the isolated nuclei in five volumes of 20 mM HEPES (pH 7.9), 1.5 mM $MgCl_2$, 0.42 M NaCl, 0.2 mM EDTA, 0.1% Triton X-100 and 25% glycerol for 30 min with gentle shaking at 4°C. The nuclei were lysed by 10 passages through an 18-gauge needle and debris was removed by centrifugation at 13 000 rpm. The supernatant served as nuclear fraction. Mitochondrial proteins were isolated by incubating the mitochondria in a hypotonic lysis buffer (10 mM HEPES, pH 7.9) for 30 min on ice, briefly sonicated and debris pelleted at 13 000 rpm for 30 min.

Trichrome Masson and senescence staining

Staining was performed on lung sections after deparaffinizing them in xylol and rehydrating them through a series of 100% ethanol, 95% ethanol, 70% ethanol then washed extensively with water and then incubated with Weigert's iron hematoxylin solution for 10 min and then, washed extensively with distilled water and incubated with Biebrich scarlet-acid fuchsin solution for 10–15 min. After incubation the slides were washed extensively and differentiated in phosphomolybdic-phosphotungstic acid solution for 10–15 min and transfer them to aniline blue solution and stain for 5–10 min. Rinse briefly in distilled water and differentiate in 1% acetic acid solution for 2–5 min. After this step slides were washed again with distilled water and dehydrated im-

mediately with 95% ethyl alcohol, absolute ethyl alcohol and *n*-xylene. The slides were then mounted and analyzed.

For detection of SA-β-gal-positive cells in lungs, cryosections of indicated lungs were made and fixed with 2% formaldehyde/0.2% glutaraldehyde/PBS for 5 min. Slides were then washed and incubated with 5-bromo-4-chloro-3-inolyl-β-d-galactoside in dimethylformamide (20 mg/ml), 40 mM sodium phosphate (pH 6.0), 5 mM potassium ferrocyanide, 5 mM potassium ferricyanide, 150 mM NaCl and 2 mM $MgCl_2$ and incubated at 37°C for 24 h. After incubation, cells/sections were washed with PBS, counter stained with eosin, mounted and imaged using an Olympus inverted microscope.

Laser micro-irradiation

Primary cells were plated on glass-bottom dishes (IBIDI μ-wells) and were pre-sensitized with 10 μM 5-bromo-2′-deoxyuridine (BrdU, Sigma-Aldrich) in phenol red-free medium (Gibco) for 24 h at 37°C. Micro-irradiation was performed with a FluoView1200 confocal microscope (Olympus Europa GmbH) equipped with an incubator (EMBL Heidelberg) heated to 37°C. A 355 nm laser (JDS Uniphase PNV-001525-0 × 0; max pulse energy 30 μJ, pulse width <500 ps) coupled in to the second scanner SIM port focused diffraction-limited through a 63×/1.35 oil objective to yield a line of 0.25–0.5μ across the nucleus. Exposure time of the micro-irradiation was 0.5 s per cell. About 60 min after the micro-irradiation treatment, cells were pre-extracted with CSK buffer and fixed with 4% paraformaldehyde for 10 min at 4°C.

Reperfusion injury

Brain. As previously described (40), mice were anesthetized with volatile anesthesia (isoflurane in $30\%O_2/70\%N_2O$) and placed in lateral position. After a skin incision between eye and ear, the temporal muscle was removed and the MCA identified. Then, a burr hole was drilled over the MCA and the dura mater was removed. The MCA was permanently occluded using bipolar electrocoagulation forceps. Permanent occlusion of the MCA was visually verified before suturing the wound. During the surgery, body temperature was maintained using a feedback-controlled heating pad.

Renal. Renal ischemia/reperfusion injury was induced as described previously (41). In WT (C57BL/6; 9–10 weeks) mice, both renal arteries were clamped for 30 min under general anesthesia inhalation anesthesia with isoflurane (Baxter, Deerfield, USA). Mice received a subcutaneous injection of 0.01mg/100g Buprenorphine (Temgesic, RB Pharmaceuticals, Berkshire, UK). Mice were sacrificed two days after I/R. Sham mice underwent the same procedure without clamping of the renal arteries.

Electrophoretic mobility shift assay

DNA RAGE or RAGE-MRE11 interaction was studied by using recombinant RAGE (and MRE11) was incubated with the labeled DNA probe, A 64 base pair probe generated by annealing two or more single stranded DNA

oligonucleotides at 95°C and allowing them to cool slowly to room temperature. For sequence details refer Supplementary Table S4 under oligo names RAGE EM-F and RAGE EM-R.

For EMSA reactions recombinant RAGE alone or in combination with MRE11 was mixed in a 20 μl reaction with 40–45 ng of probe, 0.1 mg/ml BSA and EMSA Buffer (10 mM Tris–Cl pH 7.4, 50 mM KCl, 0.5 mM MgCl$_2$, 0.1 mM EDTA, 5% glycerol) for 30 min at 25°C. Reactions were then loaded onto a pre-electrophoresed 6% acrylamide/bis (37.5:1) gel in 0.5× TBE and run at 100 V at 4°C. The gels were dried and analyzed by exposing them to photographic film.

In vitro nuclease or resectioning assay

The ϕX174 circular single-stranded virion DNA substrate (5.3 kb, New England Biolabs), was mixed with MRN or MRE11 together with BSA or RAGE in a nuclease reaction buffer (25 mM Tris–Cl (pH 7.5), 1 mM dithiothreitol, 1 mM ATP, 40 mM KCl, 10 mM NaCl and 5 mM of MgCl$_2$, 2.5 mM MnCl$_2$). After incubation for 3 h at 37°C, nuclease reactions were terminated by adding 1/10 volume of stop solution (3% SDS, 50 mM EDTA) and samples were run in a 0.8% agarose gel (1X-TAE) for 90 min at 100 mA. DNA species were stained with ethidium bromide (Promega) for 20 min and visualized by the gel dock system (Biometra).

In vitro kinase assays

In vitro kinase assays for ATM kinase were performed in 20 μl reaction volume with 1× kinase buffer (10 mM HEPES, pH 7.5, 50 mM glycerophosphate, 50 mM NaCl, 10 mM MgCl$_2$, 10 mM MnCl$_2$, 5 μM unlabeled ATP, 1 mM DTT and 5uCi γ-P^{32} ATP). To preserve the active form of ATM kinase, 0.2 μg dsDNA [pUC19 extensive sonicated DNA to yield fragments of ∼100–150 bp] was included per reaction. In each reaction tube, WT or mutant RAGE was included as substrates (1 μg/reaction) and 1 ng of the purified ATM kinase with or without purified MRN complex (100 ng/reaction) [both MRN complex and ATM was received a kind gift from Prof. Tanya Paull]. The kinase reaction was conducted at 30°C for 30 min and stopped by the addition of 1% sodium dodecyl sulfate or by adding equal volume of urea solution (6 M) and then the unincorporated label was removed by TCA precipitation of the proteins. The pellet was washed in ice cold acetone and briefly dried. The pellet was then re-suspended in 20 μl of 1× PBS and processed with Laemmli's buffer. The kinase assay products were separated on 12% SDS-PAGE. The dried gel was used for Autoradiography.

### Testing of pulmonary function

To evaluate lung mechanics, invasive lung function analysis was performed as described earlier (42), In brief mice were anesthetized with sodium pentobarbital (80 mg/kg), tracheostomized, and placed on a small animal ventilator (FlexiVent system, SCIREQ, Montreal, QC, Canada). To prevent spontaneous breathing, mice were then paralyzed with pancuronium bromide (0.5 mg/kg) and ventilated with a tidal volume of 10 ml/kg at a frequency of (150 breaths/min) and a positive end expiratory pressure of 3 cm H$_2$O to prevent alveolar collapse. Pressure–volume curves with stepwise increasing pressure (PVs–P) were consecutively measured. All perturbations were performed until three acceptable measurements were achieved.

RESULTS

RAGE deficiency affects genomic integrity and promotes cellular senescence

RAGE is known to be abundantly expressed in lungs of all vertebrates (43). To determine the cellular distribution and functional relevance of RAGE in the nucleus, lung tissue samples from wild-type (WT) mice were subjected to subcellular fractionation on a sucrose gradient. Subcellular fractionation revealed the presence of two different molecular forms of RAGE located in different sub-nuclear compartments, where the sub-form with lower molecular weight (∼50 kDa) was predominant in the soluble nuclear fraction, while the higher molecular weight (∼64 kDa) form was dominant in chromatin-associated fraction. The purity of the collected fractions was determined using specific fraction markers such as HDAC-1 to identify the soluble nuclear and histone H1 to identify the chromatin bound fraction. The antibody used was specific and did not yield a signal in RAGE$^{-/-}$ lungs (Figure 1A and Supplementary Figure S1A). This was confirmed by immunofluorescence showing a nuclear localization of RAGE (Supplementary Figure S1B). To understand the possible role of RAGE in the lung, the morphology of lungs from RAGE$^{-/-}$ mice was analyzed. The absence of RAGE was associated with an accumulation of fibrotic tissue (as evidenced by Masson's trichrome staining) and senescent lesions, as evidenced by ß-Gal-staining (Figure 1B). The accumulation of these senescent lesions was also observed in other tissues of RAGE$^{-/-}$ mice (Supplementary Figure S1C). Interestingly these changes were not associated with a specific cell type of the lung, but rather ubiquitously disseminated in a patchy pattern in all regions, encompassing all different cell types of the lungs. In addition, lungs from RAGE$^{-/-}$ mice showed a more distorted, loose pattern of alveoli and the peri-alveolar region (Figure 1B, upper panel). Consistently, these changes were also associated with a marked reduction in pulmonary function of RAGE$^{-/-}$ mice (Supplementary Figure S1D). When markers of senescence associated cellular properties were studied, an increase of IL-6 by ∼50% (Figure 1C) and an almost 3-fold increase of γH2AX and 53BP1 was seen, while pATM increased by ∼50%. This is consistent with DNA damage associated senescence and a senescence associated pro-inflammatory phenotype in cells and lungs of RAGE$^{-/-}$ mice (Figure 1C, D and Supplementary Figure S2), indicating an on-going persistent DNA damage signaling (13,14,34). The lack of adequate and timely DNA-repair may lead to the accumulation of mutations and ultimately cancer. Accordingly, long-term survival experiments showed that RAGE$^{-/-}$ mice have indeed a higher frequency of lung carcinomas as compared to WT controls (Figure 1E), indicating a change in the microenvironment of the lungs predisposing them to cancer. The increase in lung cancer became evident after 25 weeks and with increasing age, the cancer incidence rose abruptly.
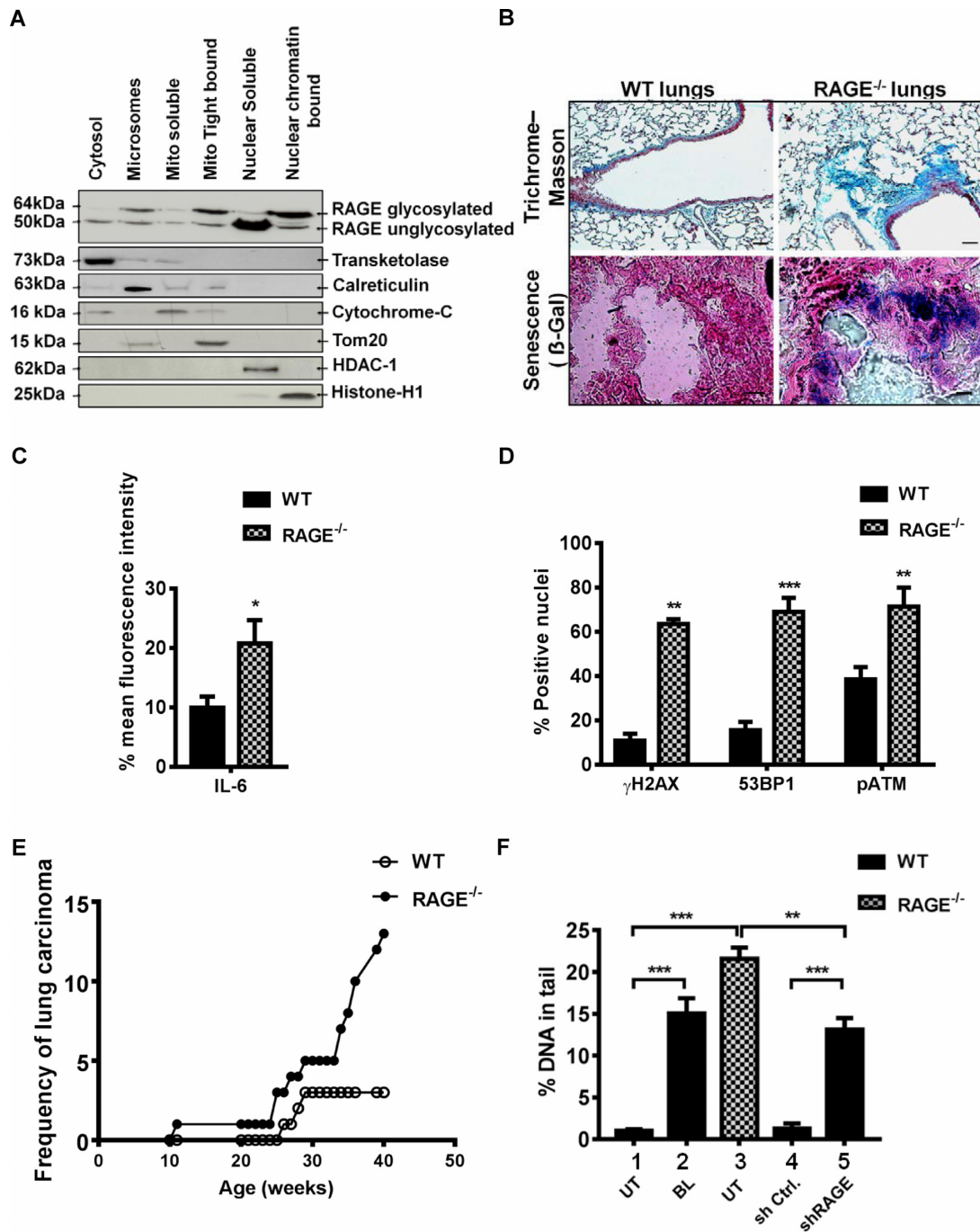
Figure 1. RAGE deficiency affects genomic integrity and promotes cellular senescence. (**A**) Representative immunoblots of WT murine lungs subjected to subcellular fractionation on a sucrose gradient as described in Materials and Methods. The supernatant was analyzed for the presence of RAGE in different fractions; particularly in nucleoplasmic, as well as the chromatin associated fraction. Here HDAC-1 or Histone-H1 antibodies were used to analyze the purity of nucleoplasmic or chromatin associated fractions respectively. Note that all fractions shows high degree of purity. (**B**) Representative images of age matched WT and affected RAGE$^{-/-}$ lung sections stained for either Masson's Trichrome stain as described in Methods (upper panel), or senescence associated β-galactosidase [β-Gal] as described in Methods (lower panel) and visualized by bright field and polarized light, where the accumulated ECM or senescent areas are recognized by its blue staining (Scale 40 μm). (**C**) Quantitative analysis of age matched WT or RAGE$^{-/-}$ lungs for persistent DNA damage associated inflammatory marker IL-6, as determined by mean fluorescence intensity of respective genotype lungs (mean ± SD, *$P < 0.05$, $N =$ 5). (**D**) Mean percentage of DSB positive nuclei (γH2AX, 53BP1 or pATM versus DAPI) in age matched WT or RAGE$^{-/-}$ lungs, as determined by immunofluorescence analysis with the respective markers (mean percentage values are represented as ± SEM, **$P < 0.01$, ***$P \leq 0.001$, $N = 5$). (**E**) The frequency of lung carcinomas determined macroscopically in WT or RAGE$^{-/-}$ mice are shown as age wise frequency distribution. Data from two independent experiments with a total of 40 mice analyzed from each group. (**F**) Quantitative analysis of DNA damage in WT or RAGE$^{-/-}$ lung fibroblasts by comet assay (average from three independent experiments, for details see Materials and Methods). Cells were either left untreated (UT; graph bar 1) or treated with Bleomycin (BL; 30 μg/ml for 60 min, graph bar 2). Untreated RAGE$^{-/-}$ cells are depicted as dotted bar (graph bar 3). WT cells treated with control shRNA (graph bar 4) were used as control for shRAGE treated WT fibroblasts (graph bar 5). The comet assay was done 60 h after transfection (mean ± SD, **$P < 0.01$, ***$P \leq 0.001$).
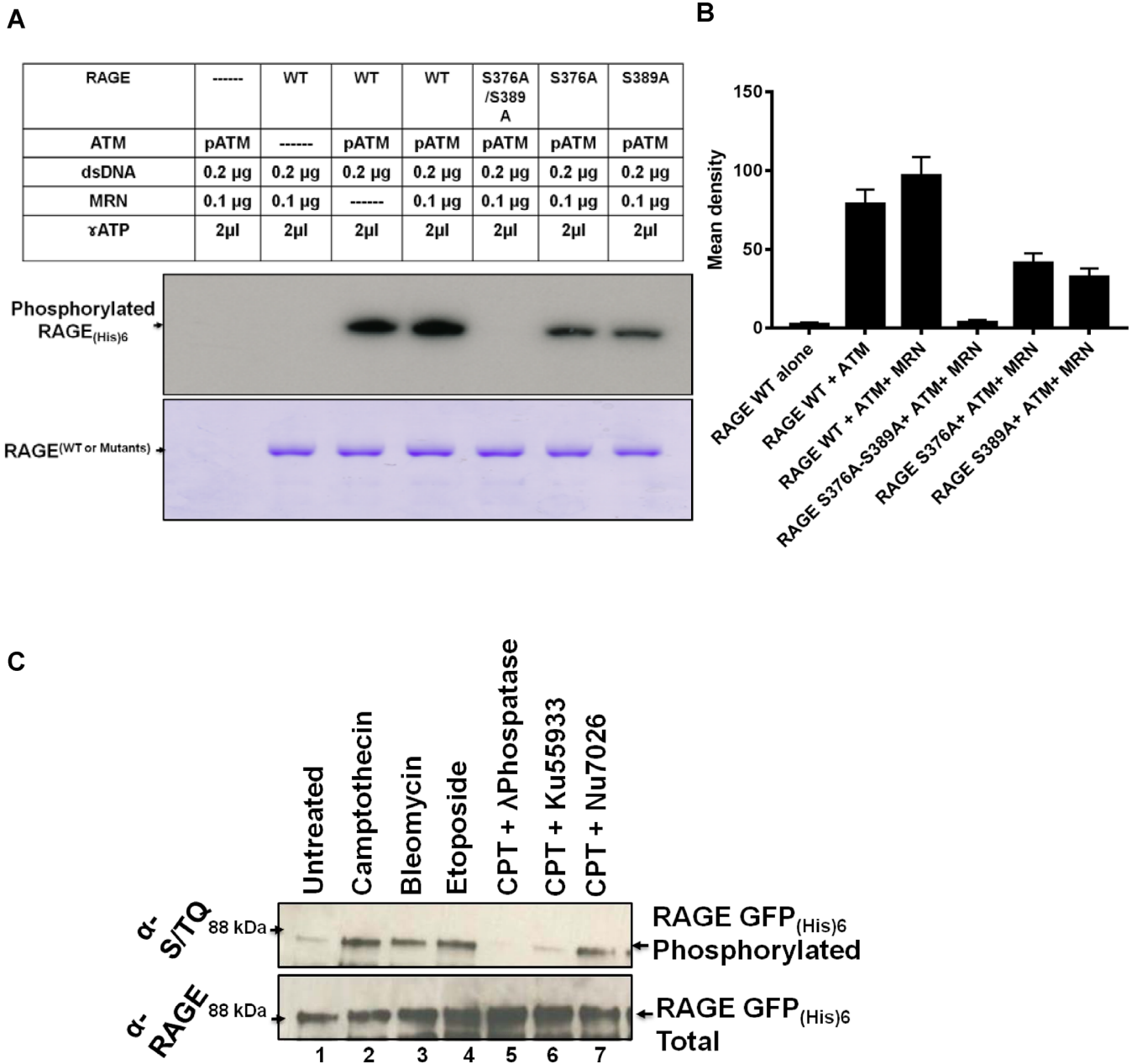
This points towards a direct or indirect link of RAGE in maintaining nuclear integrity, relevant for preventing pulmonary fibrosis and cancer.

As compared to epithelial cells, pulmonary fibroblasts are more susceptible to oxidative stress (44). Cultured pulmonary fibroblasts display a constitutive nuclear accumulation of RAGE, while A549 cells do not (Supplementary Figure S3A). Moreover, the chromatin bound RAGE can be stripped with DNase-I, but not with RNase-A further suggesting a role of RAGE in chromatin-associated functions. (Supplementary Figure S3B and S3C). The upper band is the chromatin-associated band, as shown in Figure 1A. This band is less prominent in the nuclear soluble fraction, not enhanced after RNase-A treatment, but becomes dominant in the DNase-I treated nuclear soluble fraction (Supplementary Figure S3B). Similar data was obtained when un- or pre- extracted cultured fibroblasts were stained for RAGE before and after treatment with RNase-A or DNase-I (Supplementary Figure S3C last lane, overlay). When RNase-A was added, staining remained prominent, however after DNase-I treatment, loss of RAGE staining in the overlay was evident. Moreover, co-localization studies with the nucleolar marker eIF6 or DAPI enriched heterochromatic regions (45,46) shows that RAGE does not colocalize with the nucleolar marker at the M- and G2-phase, but it shows a diffusive nucleolar localization pattern during the S-phase of the cell cycle. RAGE does not colocalize with heterochromatic foci of pulmonary fibroblasts in different stages of the cell cycle (Supplementary Figure S3D). The specificity of the DNA binding by RAGE was also validated using a gel retardation assay (Supplementary Figure S3E). When the 64mer dsDNA probe (labeled at the 5′-end) was used, the formation of a RAGE–DNA complex was observed (lane 2), which increased with increasing doses from 12.5 to 50 nM of RAGE (lanes 2–4) and was competed by excess of cold DNA (lane 5).

Consistent with the observed DSB associated phenotype in RAGE$^{-/-}$ lungs, RAGE$^{-/-}$ pulmonary fibroblasts were also found to have a several-fold higher level of broken DNA, as evidenced in the comet assay, as compared to WT controls and WT cells treated with bleomycin as positive control (Figure 1F, graph bar 1, 2 versus 3). The level of DNA damage in the WT fibroblasts could be effectively increased by transient knockdown of RAGE (Figure 1F, graph bar 4 versus 5), excluding an artifact in the RAGE$^{-/-}$ mice and cells. Furthermore, the RAGE$^{-/-}$ fibroblasts displayed a slightly reduced proliferation rate (Supplementary Figure S4A; left panel), but without much change in cell cycle profile (Supplementary Figure S4A; right panel). Their gross morphologic appearance was reminiscent of senescence, as the RAGE$^{-/-}$ cells had an *activated* morphology and enhanced cellular senescence as compared to passage matched WT cells (Supplementary Figure S4B and C). This is indicative of persistent DNA damage signaling, as well as the absence of timely DNA repair in RAGE$^{-/-}$ cells. These findings suggest that RAGE plays an integral role in preventing cellular senescence associated with loss of genomic integrity in the cell types tested.

RAGE serves as direct downstream target of DNA damage signaling mediated by an activated ATM kinase

RAGE undergoes various post-translational modifications and these modifications include glycosylation, ubiquitinylation, acetylation and phosphorylation (39,47–49). Furthermore, RAGE is known to interact with the ERK-1/2 kinase, but it cannot be phosphorylated by the ERK-1/2 kinase, as it lacks the appropriate signature motifs (50). Proteomic studies have reported conserved amino acid residues at Ser-376 and Ser-389 of murine-RAGE (accession no. NM_007425.3) as potentially phosphorylatable targets, which may be associated with the DNA damage signaling cascade. However the kinase, that performs this phosphorylation event and its functional relevance remained unknown (39,49). Since phosphorylation plays a central role in activating the cascade needed for DNA repair, RAGE *in silico* analysis was performed. The analysis predicted that these two serine (S376 and S389) residues of RAGE possess the signature motif of the ATM kinase (51). Although Serine^{389} does not reside in a canonical ATM target motif, other reports suggest the existence of a non-canonical sequence dependent phosphorylation activity of ATM kinase (52). Therefore, RAGE phosphorylation by ATM kinase was studied. ATM signaling was reconstituted *in vitro* using recombinant RAGE or its non-phosphorylatable mutants (RAGE^{S376A} or RAGE^{S389A} or RAGE$^{S376A-S389A}$). For this experiment, RAGE was expressed and purified from *Escherichia coli* cells (Supplementary Figure S4D). Unphosphorylated RAGE expressed this way is free from unwanted eukaryotic factors and can serve as phospho-acceptor in the signaling studies. In the absence of ATM, RAGE cannot become phosphorylated, but in the presence of pATM, dsDNA and [γ-^{32}p]-ATP phosphorylation occurs (Figure 2A). No signal is seen when RAGE is missing, or in the absence of ATM kinase. However, in the presence of both, a strong signal for phosphorylated RAGE becomes evident, which is even stronger in the presence of the MRN complex. When one or both phosphorylation sites were mutated, the signal intensity was either drastically reduced (RAGE^{S376A} or RAGE^{S389A}) or was completely absent (RAGE$^{S376A-S389A}$) (Figure 2A and B). To further validate the specificity of this signaling event at the cellular level, ATM–RAGE interaction was verified by co-immunoprecipitation of RAGE with the activated ATM (pATM) kinase (Supplementary Figure S4E). WT lung fibroblasts were either left untreated (Supplementary Figure S4E, lanes 1, 4 and 5) or treated with bleomycin (Supplementary Figure S4E, lanes 2, 6 and 7), or with camptothecin (Supplementary Figure S4E, lanes 3, 8 and 9). Immunoprecipitation from untreated cells, showed almost no interaction of RAGE (lower panel) and pATM (upper panel) (Supplementary Figure S4E, lane 4 and lane 5 respectively). Whereas in bleomycin or camptothecin treated cells, enrichment for pATM was seen using the anti-RAGE antibody (Supplementary Figure S4E, lane 6 and lane 8 respectively). A similar observation was made when anti-pATM (Supplementary Figure S4E, lane 7 and lane 9 respectively) antibody was used for immunoprecipitation, while no signal for either RAGE or pATM was seen using the non-specific species control antibody (Supplementary Figure S4E, lane

A

RAGE	------	WT	WT	WT	S376A/S389A	S376A	S389A
ATM	pATM	------	pATM	pATM	pATM	pATM	pATM
dsDNA	0.2 µg	0.2 µg	0.2 µg	0.2 µg	0.2 µg	0.2 µg	0.2 µg
MRN	0.1 µg	0.1 µg	------	0.1 µg	0.1 µg	0.1 µg	0.1 µg
ɣATP	2µl	2µl	2µl	2µl	2µl	2µl	2µl

B

C

Figure 2. RAGE serves as direct downstream target of DNA damage signaling mediated by an activated ATM kinase. (**A**) Approximately 1 ng of purified ATM kinase was studied in an *in vitro* kinase assay (see Materials and Methods) by using *E. coli* expressed either RAGE[WT], RAGE[S376A], RAGE[S389A] or RAGE[S376A-S389A] as phosphate acceptor. All these RAGE forms were expressed and purified simultaneously. The ATM kinase was activated by using 200 ng of extensively sonicated pUC19 DNA in each reaction. Samples were analyzed on 12% PAGE and exposed to X-ray film overnight in -80°C. The band shown represents the amount of phosphorylated RAGE. (**B**) Quantitative densitometry analysis of *in vitro* kinase assay performed as described in A. The autoradiograms were used for quantitative analysis of pATM signaling onto RAGE or its mutants ($N = 3$). (**C**) Detection of RAGE phosphorylation in WT lung fibroblasts with (α-pS/TQ-ab) 1 h after exposure to either Camptothecin (1 µM), or Bleomycin (30µg/ml), or Etoposide (5 µM), or Camptothecin with the ATM kinase specific inhibitor (Ku55933; 15 µM, 60 min before CPT treatment) or with the DNA-PK specific inhibitor (Nu7026; 10µM, 60 min before CPT treatment), added 24 h after transfection with the WT RAGE GFP-(His)6 construct. The phosphorylated RAGE was collected from the cell lysates on Ni-NTA beads followed by analyzing them by western blotting.

10), shows the specificity of this interaction assay. Thus, this data validates the previous kinase assay as well as indicates the importance of DNA damage for RAGE–pATM interaction.

In congruence, *in vitro* induction of DSBs using camptothecin, bleomycin or etoposide in cultured fibroblasts induced phosphorylation of RAGE (Figure 2C), which can only be inhibited by the ATM kinase inhibitor KU55933 (53), but not by the DNA-protein kinase (DNA-PK) specific inhibitor Nu7026 (Figure 2C). This observation was also validated in human lung adenocarcinoma cells (Supplementary Figure S4F), where the hRAGE phosphorylation at S389 can be induced by either bleomycin or camptothecin treatment (Supplementary Figure S4F, lanes 2 and 3 respectively), and mutating this residue to alanine aborts this signaling event (Supplementary Figure S4F, lanes 7–9). Further, similar to mRAGE, human RAGE phosphorylation can only be inhibited by the pATM kinase specific inhibitor, but not by a DNA-PK inhibitor (Supplementary Figure S4F, lanes 5 and 6 respectively). These data identified RAGE as a novel substrate as well as DSB dependent downstream target of the ATM kinase-signaling cascade.

RAGE is recruited to DNA DSBs foci and interacts with the MRN complex

As the ATM signaling cascade plays an important role in sequential recruitment and dynamics of repair factors during the early phases of DNA repair, any perturbation in this process affects the repair potential of the cell (54). This is consistent with the finding that endogenous RAGE accumulated and co-localized on a laser induced DNA damage strip with the different members of the MRN complex (Figure 3A). However, many proteins accumulate at laser induced damage. Therefore, the RAGE–MRN complex colocalization was also investigated in camptothecin (Supplementary Figure S5A), or bleomycin treated pulmonary fibroblasts (Supplementary Figure S5B) and in camptothecin treated human lung adenocarcinoma cells transfected with either RAGE^WT-GFP or RAGE^S376A-S389A-GFP construct (Supplementary Figure S5C). Both drugs also accumulated RAGE at damage foci as evidenced by the MRN complex subunits or γH2AX. To exclude any non-specific effect, colocalization of RAGE with the MRN complex was further verified by co-immunoprecipitation of RAGE with the MRN complex subunits (Figure 3B). WT lung fibroblasts were either left untreated (Figure 3B, lanes 1–4) or treated with bleomycin (Figure 3B, lanes 5–9). Immunoprecipitation of untreated cells using MRE11 (top), showed a weak basal interaction with RAGE (middle) and as expected for untreated cells, almost an undetectable signal with γH2AX (bottom), indicating the basal DNA damage in cultured cells. A similar observation was made using anti-RAGE for immunoprecipitation (Figure 3B, lane 3), while no signal for MRE11, RAGE or γH2AX was seen using the non-specific species control antibody (Figure 3B, lane 4). However in the bleomycin treated cells, an enrichment for RAGE and γH2AX was seen using the anti-MRE11 antibody (Figure 3B, lane 6), while the anti-RAGE (Figure 3B, lane 7) antibody enriched MRE 11 and γH2AX (compared to lane 3). The specificity of this interaction was confirmed using

ethidium bromide (Figure 3B, lane 8), which did not dissociate the complex. Thus RAGE interacts with the MRN complex and this interaction is unaided by any form of DNA. Similar data was obtained from DNA damage induced lungs. For this, mice were treated with bleomycin and the lungs were harvested after 25 h (Figure 3C). When the whole lung extract was precipitated using anti-RAGE (Figure 3C, lane 2), a clear signal for Nbs1, Rad50, MRE11 was seen. When the anti-MRE11 antibody was used (Figure 3C, lane 3), Nbs1 (Figure 3C, lane 4), RAD50 (Figure 3C, lane 5), a similar result was observed. When anti-γH2AX was used (Figure 3C, lane 6) there was also a co-precipitation of Nbs1, Rad50, MRE11 and RAGE, however the RAGE higher molecular weight band was enriched. This is consistent with our previous finding (Figure 1A), indicating that the chromatin associated higher molecular weight band is the RAGE isoform, responsible for MRE complex formation. The non-specific species control showed no interaction (Figure 3C, lane 7).

In addition to endogenous RAGE, immunoprecipitation studies were further confirmed in WT lung fibroblasts ectopically expressing different regions of RAGE. For this, cells were transfected with either RAGE-GFP, or RAGE-cyto-GFP (consisting of the cytoplasmic domain only), or GFP alone , pre-sensitised and treated with camptothecin (Supplementary Figure S5D). The first three lanes show the input controls. The GFP staining confirmed the presence of the GFP-tagged RAGE variants added (Supplementary Figure S5D, bottom). The increased GFP signal in lanes 3–6 is explained by the enrichment of the GFP-tagged proteins. A weak Rad50 (top) and MRE11 band (middle) were seen in the absence of GFP immunoprecipitations. When the lysates were precipitated with an anti-GFP antibody, recognizing either the empty vector-GFP, the GFP-RAGE or GFP-cyto-RAGE, a strong co-precipitation was seen in the cells transfected with full length (lane 4), but not, the cytoplasmic domain of RAGE (Supplementary Figure S5D, lane 5) or GFP alone (Supplementary Figure S5D, lane 6). These data show, that in cultured cells as well as in mice RAGE is involved in the complex formation occurring at the site of DNA damage. The complex consists of MRE11, Rad50, Nbs1 as well as γH2AX.

To further identify the specific subunit of the MRN complex with which RAGE interacts, a Ni-NTA pull-down assay was performed, using purified RAGE (as bait) and MRE11 (as prey)] (Figure 3D). When recombinant His-tagged RAGE was added, as strong band appeared (Figure 3D, lane 2). When MRE11 alone was added, no interaction with the Ni-NTA beads was observed, since MRE11 has no His-tag (Figure 3D, lane 3). Only a weak MRE11 signal was observed in the MRE11 blot (bottom, lane 3). While the recombinant proteins were enriched using His-tagged-RAGE in the pull down assay, using RAGE as the bait and MRE11 as the prey, a strong signal for RAGE (top), as well as MRE11 (bottom) appeared (Figure 3D, lane 4). This interaction was not blocked using DNase-I (Figure 3D, lane 5); or ethidium-bromide (Figure 3D, lane 6). Thus, RAGE directly binds MRE11 in the absence of other factors forming the MRN complex.

To understand the mechanistic specificity as well as stability of the MRE11–RAGE interaction, binding of
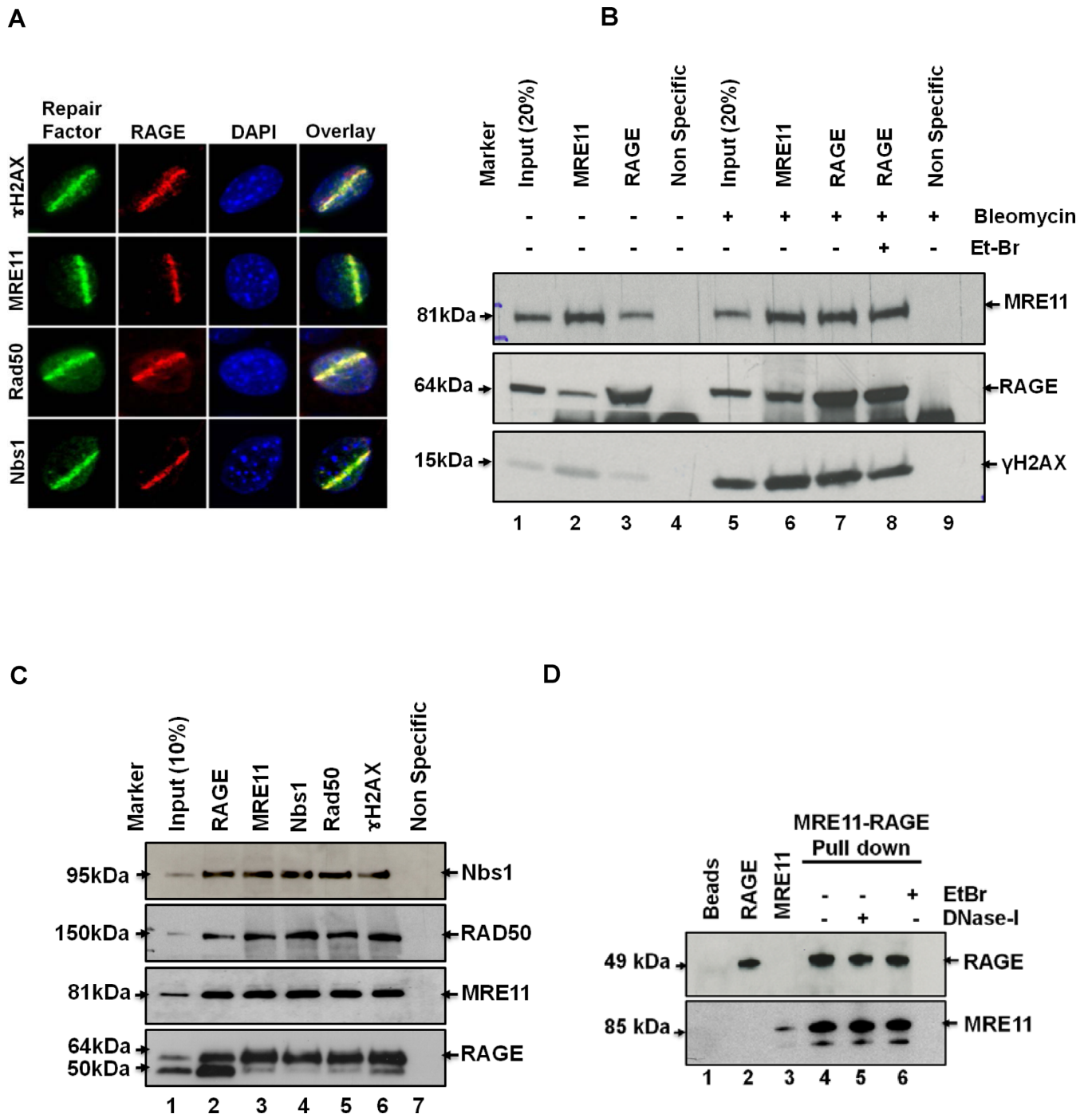
Figure 3. RAGE is recruited to DNA DSBs foci and interacts with the MRN complex. (**A**) Co-localization of RAGE with γH2AX, MRE11, Rad50 and Nbs1 to the site of laser induced DNA damage in pre-sensitized (BrdU; 10μm for 24 h in phenol red free DMEM-medium) WT lung fibroblasts, analyzed by immunofluorescence after 60 minutes of laser treatment. These cells were detergent extracted (in CSK buffer) before fixing in 4% paraformaldehyde. (**B**) Cultured pulmonary fibroblasts were pre-sensitized using BrdU (10 μM for 24 h). Cells were either left untreated or stimulated using bleomycin (30 μg/ml for 60 min). The cell extract was immunoprecipitated using antibodies against MRE11 (lanes 2 and 6), RAGE (lanes 3 and 7, 8), or a non-specific species control antibody (lanes 4 and 9). To exclude a DNA protein interaction, ethidium bromide (25 μg/ml) was added before immunoprecipitation. (**C**) Wild type mice were treated with bleomycin (2 mg/kg), after 24 h an additional boost with bleomycin (2 mg/kg) was given and 1 h later mice were sacrificed. Lungs were homogenized and a lysate was prepared as described in Materials and Methods. The input is shown in lane 1. For detection either anti-RAGE (lane 2), anti-MRE11 (lane 3), Nbs1 (lane 4), RAD50 (lane 5), γH2AX (lane 6) or non-specific species control was used (lane 7). (**D**) Using recombinant his-tagged RAGE, a Ni-NTA pull down assay was performed in Tris buffer, pH 7.5, containing 10 mM MgCl$_2$, using RAGE[(His)6] as bait and MRE11[(FLAG)] as prey. The negative control using beads alone, is shown in lane 1, RAGE alone in lane 2 and MRE11 alone in lane 3. After enrichment the pull down using his-tagged RAGE in the presence of MRE11 is shown in lane 4, the effect of DNase-I (10 U/μl, 30 min at 30°C) in lane 5, the effect of ethidium bromide (25 μg/ml) in lane 6.

either RAGE^{WT} or its non-phosphorylatable mutant (RAGE$^{S376A-S389A}$) was studied under different salt concentrations (Supplementary Figure S5E). The increasing salt (NaCl/KCl) concentrations can be used to distinguish non-specific, unstable interactions from stable and specific ones. Here, it was observed that this interaction (with either RAGE^{WT} or RAGE$^{S376A-S389A}$) was indistinguishable, when the beads were washed with low salt buffer (100mM NaCl), (Supplementary Figure S5E; lane 4 versus lane 7). However, when either 200 or 300 mM NaCl was used, binding of the RAGE$^{S376A-S389A}$, but not of RAGE^{WT}, was drastically reduced (Supplementary Figure S5E lane 5 versus lane 8; lane 6 versus lane 9). This shows that, only the RAGE^{WT} interacts stably and specifically with MRE11, whereas the RAGE$^{S376A-S389A}$ mutant not, since the RAGE^{WT} interaction with MRE11 was salt resistant.

RAGE did not co-localize with NHEJ repair foci, such as the Oct1-PTF-transcription domain, as evidenced by 53BP1 staining, in cultured pulmonary fibroblasts (Supplementary Figure S5F). Thus, RAGE has MRE11 dependent roles in recombination, but not in NHEJ repair. MRE11 possesses under normal assay conditions primarily exo-nucleolytic activities (55,56). However, in order to sustain DNA repair, MRE11 activity must be shifted from exo- to endo-nuclease activity (9,12,57). If RAGE were the factor which shifts under physiologic conditions MRE11 from exo- to endonuclease activity, than one would expect RAGE should be involved in homologous DNA repair only.

RAGE and MRE11 contribute together to end processing of the DNA and absence of RAGE affects ATM to ATR signaling

To determine the functional role of the RAGE/MRE11 interaction, the binding of RAGE purified to homogeneity and MRE11 onto the dsDNA template was studied. Super shift analysis using a native EMSA gel (non-denaturing) and purified proteins was performed in an ex vivo assay (Figure 4A). When 5′-labeled DNA was used as EMSA based probe, no shift was seen when no other protein was present (Figure 4A, lane 1). When RAGE alone was added, a shift occurred, indicating RAGE DNA binding. When MRE11 was added in increasing concentrations (Figure 4A, lanes 3–7) not only a super shift, but also a reduction in bottom band representing the labeled DNA was seen. This was also dependent on the RAGE concentration used (Figure 4A, lanes 9–13). Thus, an active complex is formed between MRE11 and RAGE on DNA, at the same time the MRE11 nuclease activity results in degradation of the DNA template used.

If the RAGE–MRE11 interaction on DNA was important for the function of MRE11, than the nucleolytic processing of the DNA ends by either the MRN complex or MRE11 should be affected by RAGE (Figure 4B). The nucleolytic activity of MRN-RAGE complex was studied using ss-circular DNA as described by Sartori *et al.* (56,58). When MRN was added alone or along with BSA (lane 2 or lane 3), very little nucleolytic activity was seen. When MRN and RAGE, were added together, a strong endonuclease activity was seen (lanes 4–7), while the addition of RAGE alone showed no nuclease activity on this template (lane 8).

Thus, RAGE in a dose dependent manner enhanced the nucleolytic processing of circular DNA. Thus in an *in vitro* reconstituted system, RAGE under normal physiological conditions [pH 7.5, ionic balance (KCl 40 mM, NaCl 10 mM) enhanced the nucleolytic activity of MRE11 nuclease.

To further prove that RAGE is actively involved in end resection activity of MRE11 nuclease, the loss of RAGE was studied with respect to other steps in the DNA repair pathway. When the effect of bleomycin was studied, the increase of pCHK1 over 24 h was evident in WT, but not in RAGE$^{-/-}$ fibroblasts, despite a normal expression of CHK1 (Figure 4C and Supplementary Figure S6A, upper panel). A similar observation was also made when WT and RAGE$^{-/-}$ cells were treated with camptothecin (Supplementary Figure S6A, lower panel and Supplementary Figure S6B). Thus, loss of RAGE did not affect the initial detection and/or signaling by ATM, resulting in normal γH2AX phosphorylation, but was associated with a lack of checkpoint kinase-1 (CHK1) phosphorylation. As phosphorylation of CHK1^{S345} is regulated by the ssDNA-RPA2 nucleoprotein sensor kinase, Ataxia telangiectasia and Rad3-related protein kinase (ATR) (59), the recruitment and phosphorylation of RPA2 bound to ssDNA was determined in cultivated pulmonary WT or RAGE$^{-/-}$ fibroblasts (Supplementary Figure S6C). When cells were treated with camptothecin (Supplementary Figure S6C, lanes 3 and 4), bleomycin (Supplementary Figure S6C, lanes 5 and 6); etoposide (Supplementary Figure S6C, lanes 7 and 8) or hydroxyurea (Supplementary Figure S6C, lanes 9 and 10), a strong phosphorylation of RPA was seen in WT, but not the RAGE$^{-/-}$ cells, despite normal total RPA, cyclin-A antigen and strong induction of γH2AX in RAGE$^{-/-}$ cells. This was confirmed by immunofluorescence staining in cultured fibroblasts (Figure 4D). Furthermore, by using a method to detect BrdU substituted cellular DNA under native (non-denaturing) conditions (60), it was observed that resection associated, BrdU substituted ssDNA foci were also absent in pre-sensitized, camptothecin treated RAGE$^{-/-}$ cells, whereas the DNA DSB formation was evident by γH2AX foci formation (Supplementary Figure S6D). Consistent with these results, RPA2 phosphorylation was also absent in lungs from RAGE$^{-/-}$ mice (Supplementary Figure S7). The absence of phosphorylated RPA2$^{S4/S8}$ foci indicated an improper end-resection of DNA, mediated by the MRN/ATR axis.

Genetic reconstitution of RAGE restores DNA repair and pulmonary function

Persistent DNA damage signaling perturbs the normal cellular homeostasis, thereby severely affecting the physiology of an organ. To validate the role of RAGE in the DSB associated senescence signaling, RAGE$^{-/-}$ cells were reconstituted with the normal, full-length RAGE (RAGE$^{1-402}$) and several RAGE mutants (Figure 5A). Compared to untreated WT cells (graph bar 1), there was a significant accumulation of broken DNA as evidenced by the comet assay in RAGE$^{-/-}$ cells (graph bar 2). This could be reduced by reconstitution of full-length wild type RAGE (graph bar 3). However, the RAGE$^{350-402}$ (graph bar 4), RAGE$^{1-235}$ (graph bar 5), or the non-phosphorylatable
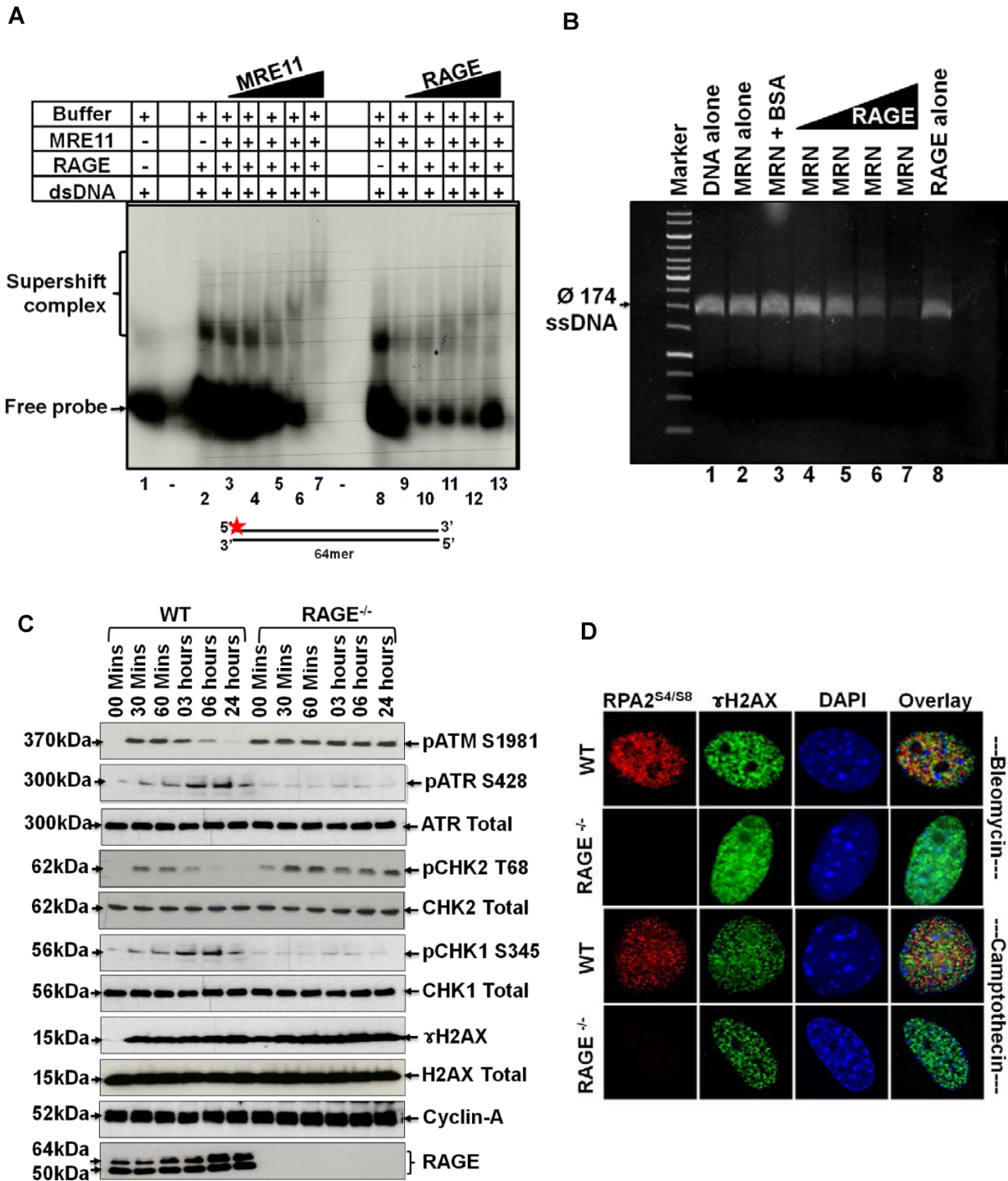
Figure 4. RAGE and MRE11 contribute together to end processing of the DNA and absence of RAGE affects ATM to ATR signaling. (**A**) Non-denaturing gel shift assay autoradiogram using dsDNA [64mer, app 40–45 ng/reaction, labeled at the 5′ end, was resolved on 6% native PAGE (20cmX20cm)]. The probe alone (lane 1), recombinant RAGE alone (0.5 μg) (lane 2) and in addition MRE11 in increasing concentrations (from 100 to 500 ng) (lanes 3–7) was added. In lanes 8–13, a constant MRE11 concentration of 0.5 μg was used, while the RAGE concentration increased from 100 to 500 ng (lanes 9–13). The DNA used is depicted below the autoradiogram (**B**) An endonuclease activity assay was performed by using a 1% agarose gel, along with the markers in lane 1. The nucleolytic processing of circular single stranded DNA derived from the viral plasmid PhiX174 was analyzed as described in Materials and Methods. Lane 2 shows the DNA alone, lane 3 in the presence of MRN alone, lane 4 MRN with BSA, lanes 5–8 in the presence of increasing amounts or RAGE as indicated. The reaction buffer contained MRN (50 nM), BSA (200 ng) or RAGE (0.4–3.2 μM) in 5 mM $MnCl_2$. (**C**) Synchronized cultured fibroblasts from WT and $RAGE^{-/-}$ lungs were treated with bleomycin (30 μg/ml for indicated times). The expression and phosphorylation status of the indicated factors was analyzed by western blotting of total extracts at the indicated times. Shown are phosphorylated CHK1 (Ser 345) and total CHK1. The cyclin-A was probed as an S-phase control, and γH2AX as a DNA DSB control. (**D**) Representative immunofluorescence images of WT or $RAGE^{-/-}$ pulmonary fibroblasts treated with either bleomycin (30 μg/ml) or camptothecin (1 μM) for 60 min, analyzed for RPA2[S4 and S8], γH2AX, DAPI and overlay. These cells were detergent extracted before fixing in 4% paraformaldehyde.
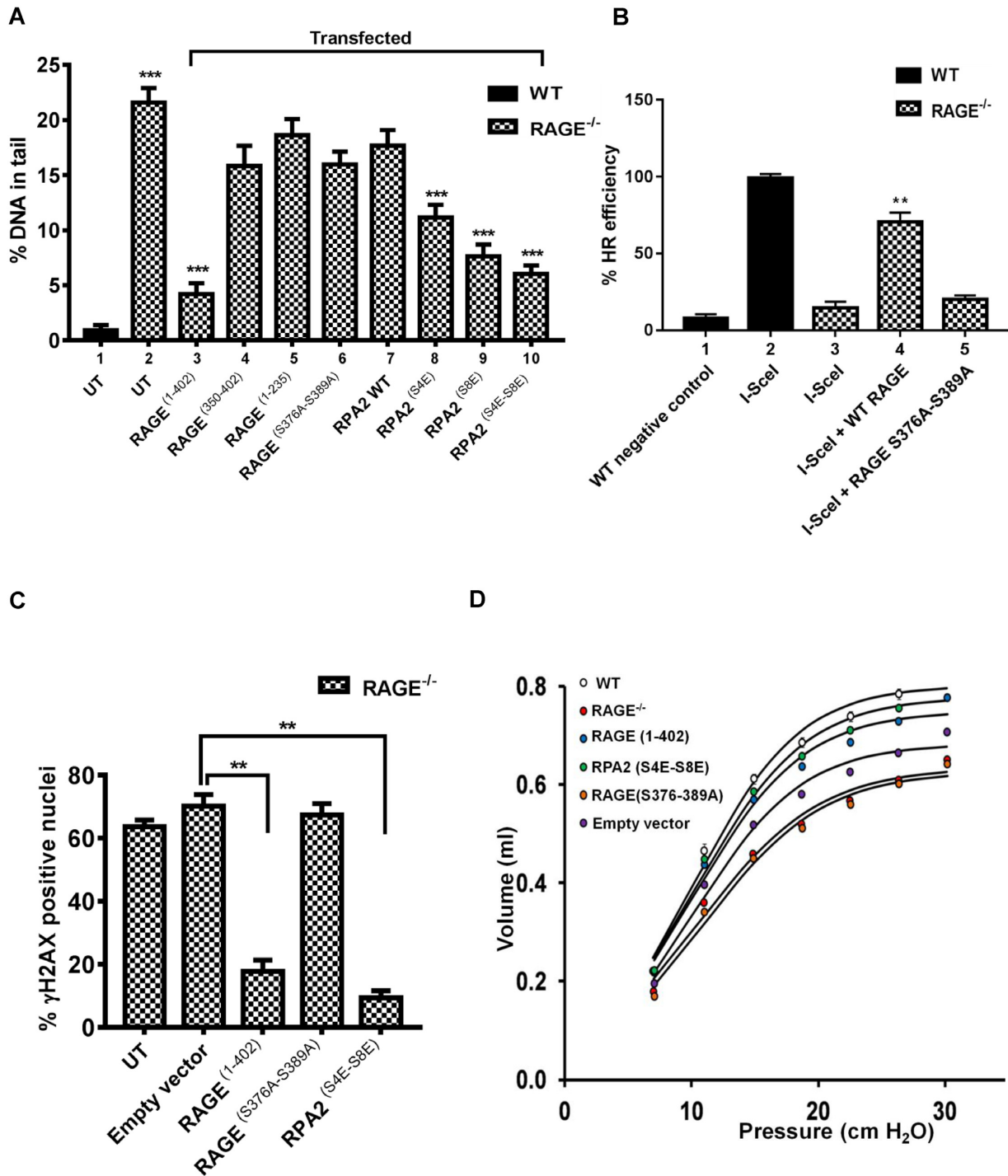
Figure 5. Genetic reconstitution of RAGE restores DNA repair and pulmonary function. (**A**) The quantitative analysis of DNA damage in WT or RAGE$^{-/-}$ lung fibroblasts was evidenced by the comet assay, as described in Materials and Methods. Cells were transiently transfected using WT full length RAGE (graph bar 3), RAGE 350–420 (graph bar 4), RAGE 1–235 (graph bar 5) or RAGE S376A/389A (graph bar 6), RPA S4E (graph bar 7), RPA S8E (graph bar 8), RPA S4E-S8E (graph bar 9). Untransfected cells served as control. Shown is the average from three independent experiments. About 100 of comets were analyzed for each construct (mean ± SEM, Student's *t*-test; ***$P \leq 0.001$). (**B**) Quantitative analysis of efficiency of recombination repair in RAGE$^{-/-}$ cells by the DR-GFP assay, as described in supplementary methods. RAGE$^{-/-}$ lung fibroblasts were transiently transfected using WT full length RAGE (graph bar 4), or RAGE S376A/389A (graph bar 5), transfected WT lung fibroblasts served as positive control (graph bar 2), untransfected cells served as negative control. Shown is the average from three independent experiments (graph bars 1 and 3). Data represents mean ± SEM (Student's *t*-test; **$P \leq 0.01$). (**C**) Quantitative analysis of γH2AX positive nuclei in lungs of RAGE$^{-/-}$ mice transduced with AAV$^{2/8}$ as described in Materials and Methods. 6-month-old mice were harvested 4 weeks after viral transduction. The empty vector served as control. Mean ± SD of six animals per group is shown (Student's *t*-test; **$P \leq 0.01$). (**D**) Pressure–volume curves were determined using the FlexiVent system in RAGE$^{-/-}$ mice, 4 weeks after transduction with the indicated virus. The curves represent group averages ($N = 6$). The lungs studied in Figure 5B and C and Supplementary Figure S9 are identical.

RAGE$^{S376A-S389A}$ or RPA2^{WT} did not reduce the level of DNA damage (graph bars 6 and 7). Furthermore the phosphomimetic mutant of RPA2 (RPA2^{S4E}, RPA2^{S8E}, RPA2$^{S4E-S8E}$ (graph bars 8–10); also reduced the DNA damage. The effect observed with the mutants of RPA2 could be the result of an indirect effect on ATR signaling and therefore allow for a RAGE-independent mode of repair in the G1-phase. Thus, ATM activated RAGE or in the absence of it, the RPA2$^{S4E–S8E}$ mediated pathway can rescue the DNA repair defect in RAGE$^{-/-}$ cells. These data are consistent with the *ex vivo* data shown above.

Furthermore, a modified DR-GFP assay was used to verify that these reconstitutions can indeed overcome the defective recombination repair system of the RAGE$^{-/-}$ (Supplementary Figure S8A). To avoid any interference from the internal GFP fluorescence (in the RAGE$^{-/-}$ mice, the RAGE gene was replaced with a GFP expression cassette; (38,61)), the DR-GFP plasmid was modified by ligating the 3X FLAG tag expressing nucleotide sequence (in frame) to the 3′-end of the SceGFP gene of the DR-GFP plasmid. This modified system was then used to analyze the repair efficiency of RAGE$^{-/-}$ lung fibroblast, which were left untransfected or transfected with either RAGE^{WT} or RAGE$^{S376A-S389A}$ constructs (Figure 5B). Furthermore, the functionality of this modified system was verified in WT pulmonary fibroblasts (Figure 5B, graph bars 1 and 2). In agreement with the previous observations in RAGE$^{-/-}$ cells, the defects associated with recombination repair can only be repaired by reconstituting RAGE^{WT}, but not by the non-phosphorylatable mutant of RAGE (RAGE$^{S376A-S389A}$). (Figure 5B, graph bar 4 versus bar 5). Since untransfected WT pulmonary fibroblasts do not express any FLAG-tagged GFP, they were used as negative control (Figure 5B, graph bar 1), WT cells transfected with modified DR-GFP as well as *i*SceI construct served as positive (100%) control (Figure 5B, graph bar 2). Since in the RAGE$^{-/-}$ cells (transfected with modified DR-GFP as well as *i*SceI construct), FLAG-GFP signal was very low (Figure 5B, graph bar 3), this indicates a defective homologous recombination repair. However, reconstitution using RAGE^{WT}, but not with RAGE$^{S376A-S389A}$ restores recombination repair (Figure 5B, graph bars 4 and 5). From these data, we conclude that RAGE stimulates end-resection and thereby promotes both ATR signaling and recombination repair.

These molecular reconstitution experiments paved the ways for clarifying the defects associated with the absence of RAGE. To understand the mechanistic link associated with the RAGE phosphorylation, an *in vitro* nuclease assay was performed by using either RAGE^{WT} or non-phosphorylatable RAGE (Supplementary Figure S8B). While RAGE^{WT} can only support the nuclease activity of the MRN complex, the mutant (RAGE$^{S376A–S389A}$) that cannot interact specifically and stably, does not support the MRN complex resection activity (Supplementary Figure S8B; lane 5 versus lane 7). Similarly the hyper-phosphorylated RAGE (RAGE$^{S376E–S389E}$; a phosphomimetic mutant of RAGE generated by replacing the serine (S) with glutamic acid (E) at the respective positions, mimics the pATM phosphorylated RAGE) supports more

efficiently the resection activity of the MRN complex (Supplementary Figure S8B; lane 5 versus lane 6). Further validates the importance of pATM-mediated phosphorylation of RAGE in end-resection.

Persistent DNA damage signaling is known to be causatively linked to idiopathic pulmonary fibrosis (IPF) (33). Similarly, RAGE$^{-/-}$ mice are considered as a model for IPF (29,36,37,62). Thus to ascertain the DNA repair associated physiological relevance of RAGE *in vivo*, RAGE expression in the lungs of RAGE$^{-/-}$ mice was reconstituted using recombinant virions (AAV2/8). Four weeks post transduction, the transduced antigen was shown to be expressed in lung tissue (Supplementary Figure S9A, upper panel). When the double strand break marker γH2AX was studied by immunofluorescence in the control and AAV treated lungs (Figure 5C), no effect of the empty vector (graph bar 2) was seen. However a significant reduction in γH2AX positive nuclei (from 63% to 18%) was seen, when the RAGE$^{-/-}$ lungs were transduced with the full-length and phosphorylatable RAGE (graph bar 3), but not with the non-phosphorylatable mutant (graph bar 4). Consistent with the RAGE mediated activation of RPA, DNA repair could also be reconstituted by transducing a phosphomimetic RPA mutant (RPA2$^{S4E–S8E}$) (graph bar 5). This was also shown using immunohistochemistry (Supplementary Figure S9A top panels) for γH2AX staining of lungs in RAGE$^{-/-}$ mice, as well as 53BP1 as marker of DNA damage (Supplementary Figure S9B). In addition, reduction in DNA damage markers was associated with a remarkable reduction in tissue fibrosis, as evidenced by decreased deposition of extracellular matrix components using Masson´s trichrome staining (Supplementary Figure S9A, lower panels). The reduction in DNA damage and fibrotic tissue corresponds well to the effect of phosphorylatable full-length RAGE treatment of pulmonary function (Figure 5D). Transduction using wild type RAGE almost normalized the pressure-volume curve to the level of healthy wild type mice, while the empty vector and non-phosphorylatable RAGE had no significant effect. Consistent with a defect in RPA phosphorylation in the absence of RAGE, an enhancement of pulmonary function was also observed in the phosphomimetic RPA transduced mice. These data provide a mechanistic link between RAGE and defective DNA-DSB repair and demonstrate the therapeutic potential of RAGE in mitigation of defective DNA-DSBs associated pulmonary fibrosis.

RAGE contributes to DNA repair in various disease models

RAGE is constitutively expressed in wide range of cell types and is up-regulated in response to oxidative challenges (63,64) as well as hypoxic stress (65). Hence, to evaluate whether nuclear RAGE is only relevant for the lung or acts as a global repair factor, murine models of hypoxia/reperfusion injury to brain or kidney (Supplementary Figure S10A) were studied. Upon hypoxia/reperfusion injury, nuclear translocation of RAGE was markedly enhanced and co-localized with γH2AX in the clamped ischemic ipsilateral brain or kidney, whilst no effect was observed in the unclamped contralateral side. In addition, in A549 cells, known to express cytoplasmic and mem-
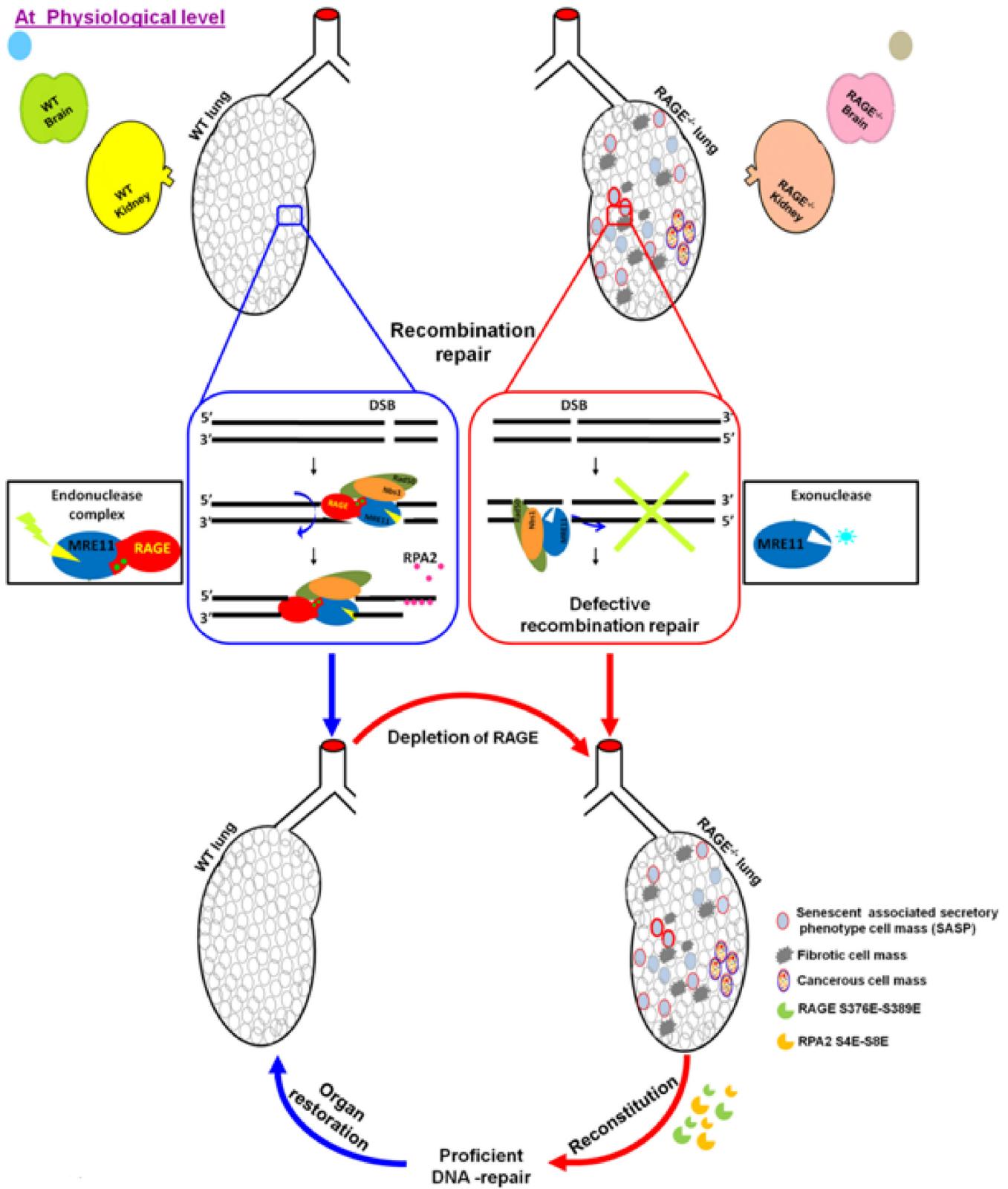
Figure 6. Schematic representation of homeostatic RAGE–ATM interaction is essential for preventing senescence-associated pulmonary fibrosis. This schematic depiction shows the importance of RAGE in timely repair of the broken ends of the DNA. Thus, RAGE plays an important role in maintaining normal homeostasis of lungs by inducing timely repair of the broken DNA.

brane RAGE, RAGE accumulates into the nucleus in these cells after induction of DSBs (Supplementary Figure S10B). Similarly, nuclear accumulation and co-localization of RAGE with γH2AX was also observed in several other cell types in response to the DNA-DSBs induced by total body irradiation in an ATM-kinase dependent manner (Supplementary Figure S11). In addition nuclear accumulation of RAGE has been shown previously in other pathological settings, which cause DNA-DSBs, such as *H. pylori* infection (66), diabetes (67) and under severe oxidative stress which affects the nuclear integrity (23–25). Thus, nuclear translocation of RAGE occurs in several pathological settings, which challenge the genomic integrity.

DISCUSSION

This study shows that RAGE can translocate to the nucleus where it accumulates in areas of DSB and becomes phosphorylated at the serines 376 and 389 by the DNA-DSB sensor kinase ‵ATM′. RAGE, physiologically abundant in the nuclei of pulmonary cells, does not control the initial DNA damage associated signaling, since ATM activation is unaffected in the absence of RAGE. RAGE by binding and tailoring the helical properties of DNA, as well as binding MRE11 via its FHA $\frac{1}{2}$ rich domain, provides a physiological template for the endorsement of MRE11 endonuclease activity. Future studies are needed to define the precise nature of the DNA binding pocket and most importantly additional factors enhancing or inhibiting RAGE–DNA interactions. Our data indicate that the native endonuclease activity of MRE11 can be enhanced by RAGE. The precise role of other endonuclease such as CtIP, in the RAGE dependent end processing remains to be studied. Nevertheless, absence of CtIP or MRE11 nucleases show a similar phenotype as the RAGE deletion shown here (56,58). The *in vitro* data indicate, that binding of DNA, ATP and MRE11 is sufficient for the endonuclease activity of the MRN complex and subsequent RPA phosphorylation on a physiologic DNA substrate. This promotes effective DNA end-resection, a process required for shuttling checkpoint activation from an ATM to an ATR dependent signaling (68). The connection between RAGE mediated MRE11 endonuclease activity and RPA function could be demonstrated by either reconstituting RAGE, or a phosphomimetic mutant of RPA. Future studies need to show, how the RAGE mediated complex formation and end processing relates to RPA phosphorylation and activity. Furthermore, not only the functional role of CtIP in this complex remains to be studied, but also the potential function of proteins known to bind RAGE, when expressed on the cell surface and also known to be present in the nucleus, such as HMGB1, members of the S100 family and others (69–72). Thus, even though the effect described here is independent of these RAGE ligands and has been demonstrated using purified proteins *ex vivo*, they may still be capable of modifying the RAGE–DNA or RAGE–MRE11 binding, by blocking regions of RAGE critical for DNA, MRE11 or ATP binding and might thus affect endorsement of the MRE11 endonuclease activity.

The function of RAGE has previously been studied with respect to its role as a transmembrane pattern recognition receptor, able to induce a sustained pro-inflammatory cellular response (21,22,72–76). This raises the question, how other cell surface factors such as Par3, MMP9, Ku, NR4A, which are involved in DSB repair too (77–79), interact with the RAGE pathway described here. In accordance with our findings, a role for nuclear receptors such as NR4A (80), TR4 (81) or surface factors (77,82) in DNA repair has also been demonstrated. Under the influence of DDR signaling (mediated by either ATM kinase or DNA-PK) (79), these receptors are translocated to the nucleus (from cell surface), co-localize with DNA damage foci and participate in DNA DSB-repair. Intriguingly, similar to the RAGE$^{-/-}$ mice, NR4A null mice also accumulate unrepaired DNA and develop cellular senescence (79), a role that is distinct from the normal functions of NR4A. Thus, not only RAGE, but also other nuclear receptors and other pattern recognition receptors (26–28) regulate DNA repair. A more generalized picture is therefore evolving, in which pattern recognition receptors are critical for DNA repair, but also participate in cell surface mediated cell activation, in most cases related to disease induction.

As is the case for many of those proteins mentioned above, the precise mechanism for nuclear localization of RAGE remains unclear. Our data show, that in all cells studied, interventions such as ischemia-reperfusion or radiation, known to induce genotoxic stress (83,84), result in nuclear translocation and co-localization of RAGE with γH2AX foci. The truncated mutant of RAGE (1–235) alone is capable of nuclear translocation, but the *in silico* analysis of this region does not identify a canonical nuclear localization signal (NLS). This observation is in agreement with recent reports, since nuclear proteomics have shown that there are many other nuclear proteins, such as ERK1/2 (85), SMAD3 (86), or MEK1 (87,88), which do not have a distinct NLS, but are nevertheless capable to translocate into the nucleus. Nuclear translocation of proteins without a NLS is mostly enabled by their direct interaction with nuclear pore complexes or shuttle proteins (89,90). In addition posttranslational modifications which affect protein stability and functionality, such as phosphorylation (91,92), SUMOylation (93), or acetylation (78) are also known to play an important role in nuclear translocation (94–96). Further mutation analysis of RAGE 1–235 may identify the minimal sequence of RAGE required for nuclear localization and might then allow to understand the mechanism of nuclear translocation. Thus, studies are needed to understand the stimulus dependent mechanisms of inducible RAGE translocation, but also the regulation of physiologic nuclear RAGE accumulation, as seen in the lung. The persistent RAGE nuclear accumulation in the lung, which is exposed to oxidative stress more than other organs under physiologic conditions, fits well to the ROS inducing stimuli, such as ischemia-reperfusion and radiation used here to induce RAGE translocation in other organs. Finally, the phenotype of RAGE$^{-/-}$ animals provides for the first time evidence for a physiologic function or RAGE (in contrast to the pathophysiologic role of cell surface RAGE in many inflammatory diseases), since RAGE$^{-/-}$ mice suffer, as a result of impaired DNA repair (97), from senescence, a senescence associated secretory phenotype and finally from pulmonary cancer and fibrosis.

Previous studies on lungs have shown that cellular senescence can be accelerated by inducing DNA damage, by targeting factors involved in DNA end-resection, or by inducing oxidative stress (98,99). Likewise, specific inhibitors, which prevent generation of endogenous DNA damage, can prevent the development of fibrosis in lungs and other organs (100), emphasizing that an efficient DNA repair system plays an important role in preventing fibrosis. RAGE$^{-/-}$ cells have a defective repair system, which abrogates timely repair of DNA, thereby directing the cellular system towards the inflammatory secretory phenotype, as also observed in persistent DNA damage signaling (14). Similarly, the absence of a functional telomere maintaining enzyme, telomerase (33,101,102), or cellular stress that generates dysfunctional telomeres (102), lead to a persistent DNA damage signaling cascade (103,104). These studies show that effective DNA repair plays an important role in preventing fibrosis. Absence of RAGE in mice compromises the effective DNA repair system and similar to the telomerase (33,101,102) and other persistent DNA damage models (105), mice lacking RAGE develop severe pulmonary fibrosis. Based on these studies, we hypothesize that defective DDR signaling, or inefficient DNA-repair mechanisms are causatively linked in RAGE$^{-/-}$ mice to chronic diseases, such as IPF or cancer. This is supported by the fact that full length RAGE, but not its ATM resistant mutants, as well as a phosphomimetic mutant of RPA, were effective in not only ensuring sufficient DNA repair, but also reversing senescence and the senescence associated secretory phenotype. This points, at least in this model, to a direct link between DNA double strand repair and senescence. However, this study not only shows the causative relationship between impaired DNA damage repair and senescence and fibrosis, but also to another consequence of senescence, namely the impairment of regenerative tissue capacity. Paracrine signaling of SASP factors, such as IL-6 (induced in the lungs of RAGE$^{-/-}$ mice) and TGF-ß, further amplify the impaired DNA damage repair by limiting the overall regenerative capacity of the lung. The current study shows, that reconstitution of RAGE reverses defective DNA repair and SASP. Most surprisingly, reintroduction of RAGE, but not its non-phosphorylatable mutant, even reverses fibrosis and normalizes in part lung function. This indicates a yet unknown cross talk between fibroblasts and their surrounding cells in pulmonary fibrosis, since the AAV serotype used, transduced fibroblasts preferentially. Whether endorsing MRE11 endonuclease activity and DNA repair accounts for the dramatic effect seen in vivo alone remains open, since RAGE not only translocates into the nucleus, but also into the mitochondria (106), recently shown to be important in the development of pulmonary fibrosis (107).

Future studies need to show how RAGE, in addition to support DNA-repair, can also induce remission of fibrosis within 4 weeks only, and how it can normalize lung function to a large extend. Nevertheless, the data shown suggest, that fibrosis might no-longer be considered a 'point of no return', since at least in this model studied, the causative link between impaired DNA repair, senescence and fibrosis can be overcome by the activity of nuclear RAGE (Figure 6). RAGE does not only promote a stop of the process leading to fibrosis, but also induces remission of fibrosis and almost normalization of lung function. Thus, a strong capacity for repair and regeneration is present even in fibrotic organs of the RAGE$^{-/-}$ mouse. Collectively, our study demonstrates an 'on-demand' repair function of RAGE, identifying a previously unsuspected function of RAGE in regulation of genome integrity.

REFERENCES

1. Jackson,S.P. and Bartek,J. (2009) The DNA-damage response in human biology and disease. *Nature*, **461**, 1071–1078.
2. Ciccia,A. and Elledge,S.J. (2010) The DNA damage response: making it safe to play with knives. *Mol. Cell*, **40**, 179–204.
3. Aparicio,T., Baer,R. and Gautier,J. (2014) DNA double-strand break repair pathway choice and cancer. *DNA Repair (Amst.)*, **19**, 169–175.
4. O'Driscoll,M. (2012) Diseases associated with defective responses to DNA damage. *Cold Spring Harb. Perspect. Biol.*, **4**, a012773.
5. Branzei,D. and Foiani,M. (2008) Regulation of DNA repair throughout the cell cycle. *Nat. Rev. Mol. Cell. Biol.*, **9**, 297–308.
6. Matsuoka,S., Ballif,B.A., Smogorzewska,A., McDonald,E.R. 3rd, Hurov,K.E., Luo,J., Bakalarski,C.E., Zhao,Z., Solimini,N., Lerenthal,Y. *et al.* (2007) ATM and ATR substrate analysis reveals extensive protein networks responsive to DNA damage. *Science*, **316**, 1160–1166.
7. Ira,G., Pellicioli,A., Balijja,A., Wang,X., Fiorani,S., Carotenuto,W., Liberi,G., Bressan,D., Wan,L., Hollingsworth,N.M. *et al.* (2004) DNA end resection, homologous recombination and DNA damage checkpoint activation require CDK1. *Nature*, **431**, 1011–1017.

8. Mimitou,E.P. and Symington,L.S. (2011) DNA end resection–unraveling the tail. *DNA Repair (Amst.)*, **10**, 344–348.

9. Cannavo,E. and Cejka,P. (2014) Sae2 promotes dsDNA endonuclease activity within Mre11-Rad50-Xrs2 to resect DNA breaks. *Nature*, **514**, 122–125.

10. Huertas,P. (2010) DNA resection in eukaryotes: deciding how to fix the break. *Nat. Struct. Mol. Biol.*, **17**, 11–16.

11. Wang,H., Li,Y., Truong,L.N., Shi,L.Z., Hwang,P.Y., He,J., Do,J., Cho,M.J., Li,H., Negrete,A. *et al.* (2014) CtIP maintains stability at common fragile sites and inverted repeats by end resection-independent endonuclease activity. *Mol. Cell*, **54**, 1012–1021.

12. Daley,J.M., Niu,H., Miller,A.S. and Sung,P. (2015) Biochemical mechanism of DSB end resection and its regulation. *DNA Repair (Amst.)*, **32**, 66–74.

13. d'Adda di Fagagna,F. (2008) Living on a break: cellular senescence as a DNA-damage response. *Nat. Rev. Cancer*, **8**, 512–522.

14. Rodier,F., Coppe,J.P., Patil,C.K., Hoeijmakers,W.A., Munoz,D.P., Raza,S.R., Freund,A., Campeau,E., Davalos,A.R. and Campisi,J. (2009) Persistent DNA damage signalling triggers senescence-associated inflammatory cytokine secretion. *Nat. Cell Biol.*, **11**, 973–979.

15. Coppe,J.P., Patil,C.K., Rodier,F., Sun,Y., Munoz,D.P., Goldstein,J., Nelson,P.S., Desprez,P.Y. and Campisi,J. (2008) Senescence-associated secretory phenotypes reveal cell-nonautonomous functions of oncogenic RAS and the p53 tumor suppressor. *PLoS Biol.*, **6**, 2853–2868.

16. Oubaha,M., Miloudi,K., Dejda,A., Guber,V., Mawambo,G., Germain,M.A., Bourdel,G., Popovic,N., Rezende,F.A., Kaufman,R.J. *et al.* (2016) Senescence-associated secretory phenotype contributes to pathological angiogenesis in retinopathy. *Sci. Transl. Med.*, **8**, 362ra144.

17. Drummond-Barbosa,D. (2008) Stem cells, their niches and the systemic environment: an aging network. *Genetics*, **180**, 1787–1797.

18. Chung,H.Y., Cesari,M., Anton,S., Marzetti,E., Giovannini,S., Seo,A.Y., Carter,C., Yu,B.P. and Leeuwenburgh,C. (2009) Molecular inflammation: underpinnings of aging and age-related diseases. *Ageing Res. Rev.*, **8**, 18–30.

19. Freund,A., Orjalo,A.V., Desprez,P.Y. and Campisi,J. (2010) Inflammatory networks during cellular senescence: causes and consequences. *Trends Mol. Med.*, **16**, 238–246.

20. Bierhaus,A., Humpert,P.M., Morcos,M., Wendt,T., Chavakis,T., Arnold,B., Stern,D.M. and Nawroth,P.P. (2005) Understanding RAGE, the receptor for advanced glycation end products. *J. Mol. Med.*, **83**, 876–886.

21. Chavakis,T., Bierhaus,A. and Nawroth,P.P. (2004) RAGE (receptor for advanced glycation end products): a central player in the inflammatory response. *Microbes Infect.*, **6**, 1219–1225.

22. Liliensiek,B., Weigand,M.A., Bierhaus,A., Nicklas,W., Kasper,M., Hofer,S., Plachky,J., Grone,H.J., Kurschus,F.C., Schmidt,A.M. *et al.* (2004) Receptor for advanced glycation end products (RAGE) regulates sepsis but not the adaptive immune response. *J. Clin. Invest.*, **113**, 1641–1650.

23. Stopper,H., Schinzel,R., Sebekova,K. and Heidland,A. (2003) Genotoxicity of advanced glycation end products in mammalian cells. *Cancer Lett.*, **190**, 151–156.

24. Mallidis,C., Agbaje,I., Rogers,D., Glenn,J., McCullough,S., Atkinson,A.B., Steger,K., Stitt,A. and McClure,N. (2007) Distribution of the receptor for advanced glycation end products in the human male reproductive tract: prevalence in men with diabetes mellitus. *Hum. Reprod.*, **22**, 2169–2177.

25. Chen,C.Y., Abell,A.M., Moon,Y.S. and Kim,K.H. (2012) An advanced glycation end product (AGE)-receptor for AGEs (RAGE) axis restores adipogenic potential of senescent preadipocytes through modulation of p53 protein function. *J. Biol. Chem.*, **287**, 44498–44507.

26. Kutikhin,A.G., Yuzhalin,A.E., Tsitko,E.A. and Brusina,E.B. (2014) Pattern recognition receptors and DNA repair: starting to put a jigsaw puzzle together. *Front. Immunol.*, **5**, 343.

27. Narayanaswamy,P.B., Tkachuk,S., Haller,H., Dumler,I. and Kiyan,Y. (2016) CHK1 and RAD51 activation after DNA damage is regulated via urokinase receptor/TLR4 signaling. *Cell Death Dis.*, **7**, e2383.

28. Harberts,E. and Gaspari,A.A. (2013) TLR signaling and DNA repair: are they associated? *J. Invest. Dermatol.*, **133**, 296–302.

29. Chavakis,T., Bierhaus,A., Al-Fakhri,N., Schneider,D., Witte,S., Linn,T., Nagashima,M., Morser,J., Arnold,B., Preissner,K.T. *et al.* (2003) The pattern recognition receptor (RAGE) is a counterreceptor for leukocyte integrins: a novel pathway for inflammatory cell recruitment. *J. Exp. Med.*, **198**, 1507–1515.

30. Moding,E.J., Lee,C.L., Castle,K.D., Oh,P., Mao,L., Zha,S., Min,H.D., Ma,Y., Das,S. and Kirsch,D.G. (2014) Atm deletion with dual recombinase technology preferentially radiosensitizes tumor endothelium. *J. Clin. Invest.*, **124**, 3325–3338.

31. Schroeder,S.A., Swift,M., Sandoval,C. and Langston,C. (2005) Interstitial lung disease in patients with ataxia-telangiectasia. *Pediatric Pulmonol.*, **39**, 537–543.

32. Armanios,M. (2012) Telomerase mutations and the pulmonary fibrosis-bone marrow failure syndrome complex. *N. Engl. J. Med.*, **367**, 384.

33. Povedano,J.M., Martinez,P., Flores,J.M., Mulero,F. and Blasco,M.A. (2015) Mice with pulmonary fibrosis driven by telomere dysfunction. *Cell Rep.*, **12**, 286–299.

34. Svegliati,S., Marrone,G., Pezone,A., Spadoni,T., Grieco,A., Moroncini,G., Grieco,D., Vinciguerra,M., Agnese,S., Jungel,A. *et al.* (2014) Oxidative DNA damage induces the ATM-mediated transcriptional suppression of the Wnt inhibitor WIF-1 in systemic sclerosis and fibrosis. *Sci. Signal.*, **7**, ra84.

35. Ruzankina,Y., Pinzon-Guzman,C., Asare,A., Ong,T., Pontano,L., Cotsarelis,G., Zediak,V.P., Velez,M., Bhandoola,A. and Brown,E.J. (2007) Deletion of the developmentally essential gene ATR in adult mice leads to age-related phenotypes and stem cell loss. *Cell Stem Cell*, **1**, 113–126.

36. Englert,J.M., Kliment,C.R., Ramsgaard,L., Milutinovic,P.S., Crum,L., Tobolewski,J.M. and Oury,T.D. (2011) Paradoxical function for the receptor for advanced glycation end products in mouse models of pulmonary fibrosis. *Int. J. Clin. Exp. Pathol.*, **4**, 241–254.

37. Englert,J.M., Hanford,L.E., Kaminski,N., Tobolewski,J.M., Tan,R.J., Fattman,C.L., Ramsgaard,L., Richards,T.J., Loutaev,I., Nawroth,P.P. *et al.* (2008) A role for the receptor for advanced glycation end products in idiopathic pulmonary fibrosis. *Am. J. Pathol.*, **172**, 583–591.

38. Constien,R., Forde,A., Liliensiek,B., Grone,H.J., Nawroth,P., Hammerling,G. and Arnold,B. (2001) Characterization of a novel EGFP reporter mouse to monitor Cre recombination as demonstrated by a Tie2 Cre mouse line. *Genesis*, **30**, 36–44.

39. Cox,B. and Emili,A. (2006) Tissue subcellular fractionation and protein extraction for use in mass-spectrometry-based proteomics. *Nat. Protoc.*, **1**, 1872–1878.

40. Llovera,G., Roth,S., Plesnila,N., Veltkamp,R. and Liesz,A. (2014) Modeling stroke in mice: permanent coagulation of the distal middle cerebral artery. *J. Vis. Exp.*, e51729.

41. Dessing,M.C., Pulskens,W.P., Teske,G.J., Butter,L.M., van der Poll,T., Yang,H., Tracey,K.J., Nawroth,P.P., Bierhaus,A., Florquin,S. *et al.* (2012) RAGE does not contribute to renal injury and damage upon ischemia/reperfusion-induced injury. *J. Innate Immun.*, **4**, 80–85.

42. Wielputz,M.O., Eichinger,M., Zhou,Z., Leotta,K., Hirtz,S., Bartling,S.H., Semmler,W., Kauczor,H.U., Puderbach,M. and Mall,M.A. (2011) In vivo monitoring of cystic fibrosis-like lung disease in mice by volumetric computed tomography. *Eur. Respir. J.*, **38**, 1060–1070.

43. Katsuoka,F., Kawakami,Y., Arai,T., Imuta,H., Fujiwara,M., Kanma,H. and Yamashita,K. (1997) Type II alveolar epithelial cells in lung express receptor for advanced glycation end products (RAGE) gene. *Biochem. Biophys. Res. Commun.*, **238**, 512–516.

44. Tkaczyk,J. and Vizek,M. (2007) Oxidative stress in the lung tissue–sources of reactive oxygen species and antioxidant defence. *Prague Med. Rep.*, **108**, 105–114.

45. Miluzio,A., Beugnet,A., Volta,V. and Biffo,S. (2009) Eukaryotic initiation factor 6 mediates a continuum between 60S ribosome biogenesis and translation. *EMBO Rep.*, **10**, 459–465.

46. Zhang,K., Gao,Y., Li,J., Burgess,R., Han,J., Liang,H., Zhang,Z. and Liu,Y. (2016) A DNA binding winged helix domain in CAF-1 functions with PCNA to stabilize CAF-1 at replication forks. *Nucleic Acids Res.*, **44**, 5083–5094.

47. Park,S.J., Kleffmann,T. and Hessian,P.A. (2011) The G82S polymorphism promotes glycosylation of the receptor for advanced glycation end products (RAGE) at asparagine 81: comparison of wild-type rage with the G82S polymorphic variant. *J. Biol. Chem.*, **286**, 21384–21392.

48. Lundby,A., Lage,K., Weinert,B.T., Bekker-Jensen,D.B., Secher,A., Skovgaard,T., Kelstrup,C.D., Dmytriyev,A., Choudhary,C., Lundby,C. *et al.* (2012) Proteomic analysis of lysine acetylation sites in rat tissues reveals organ specificity and subcellular patterns. *Cell Rep.*, **2**, 419–431.

49. Elia,A.E., Boardman,A.P., Wang,D.C., Huttlin,E.L., Everley,R.A., Dephoure,N., Zhou,C., Koren,I., Gygi,S.P. and Elledge,S.J. (2015) Quantitative proteomic atlas of ubiquitination and acetylation in the DNA damage response. *Mol. Cell*, **59**, 867–881.

50. Ishihara,K., Tsutsumi,K., Kawane,S., Nakajima,M. and Kasaoka,T. (2003) The receptor for advanced glycation end-products (RAGE) directly binds to ERK by a D-domain-like docking site. *FEBS Lett.*, **550**, 107–113.

51. Mitchell,A. (2001) Motif with a motive. *Nat. Rev. Mol. Cell. Biol.*, **2**, 87.

52. Kodama,M., Otsubo,C., Hirota,T., Yokota,J., Enari,M. and Taya,Y. (2010) Requirement of ATM for rapid p53 phosphorylation at Ser46 without Ser/Thr-Gln sequences. *Mol. Cell. Biol.*, **30**, 1620–1633.

53. Hickson,I., Zhao,Y., Richardson,C.J., Green,S.J., Martin,N.M., Orr,A.I., Reaper,P.M., Jackson,S.P., Curtin,N.J. and Smith,G.C. (2004) Identification and characterization of a novel and specific inhibitor of the ataxia-telangiectasia mutated kinase ATM. *Cancer Res.*, **64**, 9152–9159.

54. Demonacos,C., Krstic-Demonacos,M., Smith,L., Xu,D., O'Connor,D.P., Jansson,M. and La Thangue,N.B. (2004) A new effector pathway links ATM kinase with the DNA damage response. *Nat. Cell Biol.*, **6**, 968–976.

55. Paull,T.T. and Gellert,M. (1998) The 3′ to 5′ exonuclease activity of Mre 11 facilitates repair of DNA double-strand breaks. *Mol. Cell*, **1**, 969–979.

56. Shibata,A., Moiani,D., Arvai,A.S., Perry,J., Harding,S.M., Genois,M.M., Maity,R., van Rossum-Fikkert,S., Kertokalio,A., Romoli,F. *et al.* (2014) DNA double-strand break repair pathway choice is directed by distinct MRE11 nuclease activities. *Mol. Cell*, **53**, 7–18.

57. Deshpande,R.A., Lee,J.H., Arora,S. and Paull,T.T. (2016) Nbs1 converts the human Mre11/Rad50 nuclease complex into an endo/exonuclease machine specific for protein-DNA adducts. *Mol. Cell*, **64**, 593–606.

58. Sartori,A.A., Lukas,C., Coates,J., Mistrik,M., Fu,S., Bartek,J., Baer,R., Lukas,J. and Jackson,S.P. (2007) Human CtIP promotes DNA end resection. *Nature*, **450**, 509–514.

59. Olson,E., Nievera,C.J., Klimovich,V., Fanning,E. and Wu,X. (2006) RPA2 is a direct downstream target for ATR to regulate the S-phase checkpoint. *J. Biol. Chem.*, **281**, 39517–39533.

60. Raderschall,E., Golub,E.I. and Haaf,T. (1999) Nuclear foci of mammalian recombination proteins are located at single-stranded DNA regions formed after DNA damage. *Proc. Natl. Acad. Sci. U.S.A.*, **96**, 1921–1926.

61. Pierce,A.J., Johnson,R.D., Thompson,L.H. and Jasin,M. (1999) XRCC3 promotes homology-directed repair of DNA damage in mammalian cells. *Genes Dev.*, **13**, 2633–2638.

62. B,B.M., Lawson,W.E., Oury,T.D., Sisson,T.H., Raghavendran,K. and Hogaboam,C.M. (2013) Animal models of fibrotic lung disease. *Am. J. Respir. Cell Mol. Biol.*, **49**, 167–179.

63. Li,J. and Schmidt,A.M. (1997) Characterization and functional analysis of the promoter of RAGE, the receptor for advanced glycation end products. *J. Biol. Chem.*, **272**, 16498–16506.

64. Schmidt,A.M., Yan,S.D., Yan,S.F. and Stern,D.M. (2001) The multiligand receptor RAGE as a progression factor amplifying immune and inflammatory responses. *J. Clin. Invest.*, **108**, 949–955.

65. Lee,J.C., Cho,J.H., Cho,G.S., Ahn,J.H., Park,J.H., Kim,I.H., Cho,J.H., Tae,H.J., Cheon,S.H., Ahn,J.Y. *et al.* (2014) Effect of transient cerebral ischemia on the expression of receptor for advanced glycation end products (RAGE) in the gerbil hippocampus proper. *Neurochem. Res.*, **39**, 1553–1563.

66. Morales,M.E., Rojas,R.A., Monasterio,A.V., Gonzalez,B.I., Figueroa,C.I., Manques,M.B., Romero,E.J., Llanos,L.J., Valdes,M.E. and Cofre,L.C. (2013) [Expression of RAGE in Helicobacter pylori infested gastric biopsies]. *Rev. Med. Chil.*, **141**, 1240–1248.

67. Karimi,J., Goodarzi,M.T., Tavilani,H., Khodadadi,I. and Amiri,I. (2012) Increased receptor for advanced glycation end products in spermatozoa of diabetic men and its association with sperm nuclear DNA fragmentation. *Andrologia*, **44**(Suppl. 1), 280–286.

68. Zhao,H. and Piwnica-Worms,H. (2001) ATR-mediated checkpoint pathways regulate phosphorylation and activation of human Chk1. *Mol. Cell. Biol.*, **21**, 4129–4139.

69. Leclerc,E., Fritz,G., Vetter,S.W. and Heizmann,C.W. (2009) Binding of S100 proteins to RAGE: an update. *Biochim. Biophys. Acta*, **1793**, 993–1007.

70. Gorsler,T., Murzik,U., Ulbricht,T., Hentschel,J., Hemmerich,P. and Melle,C. (2010) DNA damage-induced translocation of S100A11 into the nucleus regulates cell proliferation. *BMC Cell Biol.*, **11**, 100.

71. Pusterla,T., de Marchis,F., Palumbo,R. and Bianchi,M.E. (2009) High mobility group B2 is secreted by myeloid cells and has mitogenic and chemoattractant activities similar to high mobility group B1. *Autoimmunity*, **42**, 308–310.

72. Ramasamy,R., Yan,S.F. and Schmidt,A.M. (2011) Receptor for AGE (RAGE): signaling mechanisms in the pathogenesis of diabetes and its complications. *Ann. N. Y. Acad. Sci.*, **1243**, 88–102.

73. Bierhaus,A. and Nawroth,P.P. (2009) Multiple levels of regulation determine the role of the receptor for AGE (RAGE) as common soil in inflammation, immune responses and diabetes mellitus and its complications. *Diabetologia*, **52**, 2251–2263.

74. Frommhold,D., Kamphues,A., Hepper,I., Pruenster,M., Lukic,I.K., Socher,I., Zablotskaya,V., Buschmann,K., Lange-Sperandio,B., Schymeinsky,J. *et al.* (2010) RAGE and ICAM-1 cooperate in mediating leukocyte recruitment during acute inflammation in vivo. *Blood*, **116**, 841–849.

75. Bierhaus,A., Haslbeck,K.M., Humpert,P.M., Liliensiek,B., Dehmer,T., Morcos,M., Sayed,A.A., Andrassy,M., Schiekofer,S., Schneider,J.G. *et al.* (2004) Loss of pain perception in diabetes is dependent on a receptor of the immunoglobulin superfamily. *J. Clin. Invest.*, **114**, 1741–1751.

76. Sparvero,L.J., Asafu-Adjei,D., Kang,R., Tang,D., Amin,N., Im,J., Rutledge,R., Lin,B., Amoscato,A.A., Zeh,H.J. *et al.* (2009) RAGE (Receptor for Advanced Glycation Endproducts), RAGE ligands, and their role in cancer and inflammation. *J. Transl. Med.*, **7**, 17.

77. Monferran,S., Paupert,J., Dauvillier,S., Salles,B. and Muller,C. (2004) The membrane form of the DNA repair protein Ku interacts at the cell surface with metalloproteinase 9. *EMBO J.*, **23**, 3758–3768.

78. Li,T., Diner,B.A., Chen,J. and Cristea,I.M. (2012) Acetylation modulates cellular distribution and DNA sensing ability of interferon-inducible protein IFI16. *Proc. Natl. Acad. Sci. U.S.A.*, **109**, 10558–10563.

79. Malewicz,M., Kadkhodaei,B., Kee,N., Volakakis,N., Hellman,U., Viktorsson,K., Leung,C.Y., Chen,B., Lewensohn,R., van Gent,D.C. *et al.* (2011) Essential role for DNA-PK-mediated phosphorylation of NR4A nuclear orphan receptors in DNA double-strand break repair. *Genes Dev.*, **25**, 2031–2040.

80. Schuldt,A. (2011) DNA repair: Nuclear receptors in repair. *Nat. Rev. Mol. Cell Biol.*, **12**, 690.

81. Lin,S.J., Lee,S.O., Lee,Y.F., Miyamoto,H., Yang,D.R., Li,G. and Chang,C. (2014) TR4 nuclear receptor functions as a tumor suppressor for prostate tumorigenesis via modulation of DNA damage/repair system. *Carcinogenesis*, **35**, 1399–1406.

82. Lee,J.H. and Paull,T.T. (2007) Activation and regulation of ATM kinase activity in response to DNA double-strand breaks. *Oncogene*, **26**, 7741–7748.

83. Jin,K., Chen,J., Nagayama,T., Chen,M., Sinclair,J., Graham,S.H. and Simon,R.P. (1999) In situ detection of neuronal DNA strand breaks using the Klenow fragment of DNA polymerase I reveals different mechanisms of neuron death after global cerebral ischemia. *J. Neurochem.*, **72**, 1204–1214.

84. Xia,Z., Chen,Y., Fan,Q. and Xue,M. (2014) Oxidative stress-mediated reperfusion injury: mechanism and therapies. *Oxid. Med. Cell Longev.*, **2014**, 373081.

85. Chuderland,D., Konson,A. and Seger,R. (2008) Identification and characterization of a general nuclear translocation signal in signaling proteins. *Mol. Cell*, **31**, 850–861.

86. Xu,L., Alarcon,C., Col,S. and Massague,J. (2003) Distinct domain utilization by Smad3 and Smad4 for nucleoporin interaction and nuclear import. *J. Biol. Chem.*, **278**, 42569–42577.

87. Chen,R.H., Sarnecki,C. and Blenis,J. (1992) Nuclear localization and regulation of erk- and rsk-encoded protein kinases. *Mol. Cell. Biol.*, **12**, 915–927.

88. Jaaro,H., Rubinfeld,H., Hanoch,T. and Seger,R. (1997) Nuclear translocation of mitogen-activated protein kinase kinase (MEK1) in response to mitogenic stimulation. *Proc. Natl. Acad. Sci. U.S.A.*, **94**, 3742–3747.

89. Fagotto,F., Gluck,U. and Gumbiner,B.M. (1998) Nuclear localization signal-independent and importin/karyopherin-independent nuclear import of beta-catenin. *Curr. Biol.*, **8**, 181–190.

90. Chen,X. and Xu,L. (2010) Specific nucleoporin requirement for Smad nuclear translocation. *Mol. Cell. Biol.*, **30**, 4022–4034.

91. Harreman,M.T., Kline,T.M., Milford,H.G., Harben,M.B., Hodel,A.E. and Corbett,A.H. (2004) Regulation of nuclear import by phosphorylation adjacent to nuclear localization signals. *J. Biol. Chem.*, **279**, 20613–20621.

92. Hagting,A., Jackman,M., Simpson,K. and Pines,J. (1999) Translocation of cyclin B1 to the nucleus at prophase requires a phosphorylation-dependent nuclear import signal. *Curr. Biol.*, **9**, 680–689.

93. Lin,X., Liang,M., Liang,Y.Y., Brunicardi,F.C. and Feng,X.H. (2003) SUMO-1/Ubc9 promotes nuclear accumulation and metabolic stability of tumor suppressor Smad4. *J. Biol. Chem.*, **278**, 31043–31048.

94. Burgon,P.G., Lee,W.L., Nixon,A.B., Peralta,E.G. and Casey,P.J. (2001) Phosphorylation and nuclear translocation of a regulator of G protein signaling (RGS10). *J. Biol. Chem.*, **276**, 32828–32834.

95. Huq,M.D. and Wei,L.N. (2005) Post-translational modification of nuclear co-repressor receptor-interacting protein 140 by acetylation. *Mol. Cell Proteomics*, **4**, 975–983.

96. Sehat,B., Tofigh,A., Lin,Y., Trocme,E., Liljedahl,U., Lagergren,J. and Larsson,O. (2010) SUMOylation mediates the nuclear translocation and signaling of the IGF-1 receptor. *Sci. Signal.*, **3**, ra10.

97. Aoshiba,K., Tsuji,T., Kameyama,S., Itoh,M., Semba,S., Yamaguchi,K. and Nakamura,H. (2013) Senescence-associated secretory phenotype in a mouse model of bleomycin-induced lung injury. *Exp. Toxicol. Pathol.*, **65**, 1053–1062.

98. Kaidi,A., Weinert,B.T., Choudhary,C. and Jackson,S.P. (2010) Human SIRT6 promotes DNA end resection through CtIP deacetylation. *Science*, **329**, 1348–1353.

99. Minagawa,S., Araya,J., Numata,T., Nojiri,S., Hara,H., Yumino,Y., Kawaishi,M., Odaka,M., Morikawa,T., Nishimura,S.L. *et al.* (2011) Accelerated epithelial cell senescence in IPF and the inhibitory role of SIRT6 in TGF-beta-induced senescence of human bronchial epithelial cells. *Am. J. Physiol. Lung Cell Mol. Physiol.*, **300**, L391–L401.

100. Hecker,L., Logsdon,N.J., Kurundkar,D., Kurundkar,A., Bernard,K., Hock,T., Meldrum,E., Sanders,Y.Y. and Thannickal,V.J. (2014) Reversal of persistent fibrosis in aging by targeting Nox4-Nrf2 redox imbalance. *Sci. Transl. Med.*, **6**, 231ra247.

101. Tsakiri,K.D., Cronkhite,J.T., Kuan,P.J., Xing,C., Raghu,G., Weissler,J.C., Rosenblatt,R.L., Shay,J.W. and Garcia,C.K. (2007) Adult-onset pulmonary fibrosis caused by mutations in telomerase. *Proc. Natl. Acad. Sci. U.S.A.*, **104**, 7552–7557.

102. Armanios,M. (2012) Telomerase and idiopathic pulmonary fibrosis. *Mutat. Res.*, **730**, 52–58.

103. Longhese,M.P. (2008) DNA damage response at functional and dysfunctional telomeres. *Genes Dev.*, **22**, 125–140.

104. Fumagalli,M., Rossiello,F., Clerici,M., Barozzi,S., Cittaro,D., Kaplunov,J.M., Bucci,G., Dobreva,M., Matti,V., Beausejour,C.M. *et al.* (2012) Telomeric DNA damage is irreparable and causes persistent DNA-damage-response activation. *Nat. Cell Biol.*, **14**, 355–365.

105. Yang,S.F., Chang,C.W., Wei,R.J., Shiue,Y.L., Wang,S.N. and Yeh,Y.T. (2014) Involvement of DNA damage response pathways in hepatocellular carcinoma. *BioMed Res. Int.*, **2014**, 153867.

106. Kang,R., Tang,D., Schapiro,N.E., Loux,T., Livesey,K.M., Billiar,T.R., Wang,H., Van Houten,B., Lotze,M.T. and Zeh,H.J. (2014) The HMGB1/RAGE inflammatory pathway promotes pancreatic tumor growth by regulating mitochondrial bioenergetics. *Oncogene*, **33**, 567–577.

107. Mora,A.L., Bueno,M. and Rojas,M. (2017) Mitochondria in the spotlight of aging and idiopathic pulmonary fibrosis. *J. Clin. Invest.*, **127**, 405–414.